Directed evolution-based discovery of ligands for in vivo restimulation of CAR-T cells

Authors: Tomasz M. Grzywa[1], Alexandra Neeser[1,2#], Ranjani Ramasubramanian[1,2#], Anna Romanov[11,13], Ryan Tannir[1, 3], Naveen K. Mehta[11], Benjamin Cossette[11], Duncan M. Morgan[11,14], Beatriz Goncalves[1,4], Ina Sukaj[11], Elisa Bergaggio[17], Stephan Kadauke[5], Regina M. Myers[9,10], Luca Paruzzo[6,7,8], Guido Ghilardi[6,7,8], Austin Cozzone[1], Stephen J. Schuster[7,8], Noelle Frey[7,8], Libin Zhang[11], Parisa Yousefpour[11], Wuhbet Abraham[11], Heikyung Suh[11], Marco Ruella[6,7,8], Stephan A. Grupp[5,9,10], Roberto Chiarle[17,18], K. Dane Wittrup[11,13,14], Leyuan Ma[1,5,6,8,11]*, Darrell J. Irvine[11,12,13,15,16]*

Affiliations:

[1]The Raymond G. Perelman Center for Cellular and Molecular Therapeutics, Children's Hospital of Philadelphia, Philadelphia, PA 19104, USA

[2]Department of Bioengineering, School of Engineering and Applied Science, University of Pennsylvania, Philadelphia, PA 19104, USA

[3]College of Arts and Sciences, University of Pennsylvania, Philadelphia, PA 19104, USA

[4]Department of Cancer Biology, Perelman School of Medicine, University of Pennsylvania, Philadelphia, PA 19104, USA.

[5]Department of Pathology and Laboratory Medicine, Perelman School of Medicine, University of Pennsylvania, Philadelphia, PA 19104, USA.

[6]Center for Cellular Immunotherapies, University of Pennsylvania, Philadelphia, PA 19104, USA

[7]Division of Hematology/Oncology, University of Pennsylvania Perelman School of Medicine, Philadelphia, PA 19104, USA

[8]Abramson Cancer Center, University of Pennsylvania, Philadelphia, PA 19104, USA

[9]Division of Oncology, Department of Pediatrics, Perelman School of Medicine, University of Pennsylvania, Philadelphia, PA

[10]Cellular Therapy and Transplant Section and Cancer Immunotherapy Program, Children's Hospital of Philadelphia, Philadelphia, PA 19104, USA

[11]David H. Koch Institute for Integrative Cancer Research, MIT, Cambridge, MA, 02139, USA.

[12]Department of Materials Science and Engineering, MIT, Cambridge, MA, 02139, USA.

[13]Department of Biological Engineering, MIT, Cambridge, MA, 02139, USA.

[14]Department of Chemical Engineering, MIT, Cambridge, MA, USA.

[15]Ragon Institute of Massachusetts General Hospital, Cambridge, MA, 02139, USA.

[16]Howard Hughes Medical Institute, Chevy Chase, MD, 20815, USA.

[17]Department of Pathology, Boston Children's Hospital and Harvard Medical School, Boston, MA 02115, USA

[18]Department of Molecular Biotechnology and Health Sciences, University of Torino, 10126 Torino, Italy

[#] These authors contributed equally

* Correspondence: Leyuan.ma@pennmedicine.upenn.edu (L.M.), djirvine@mit.edu (D.J.I)

Abstract

Chimeric antigen receptor (CAR) T cell therapy targeting CD19 elicits remarkable clinical efficacy in B-cell malignancies, but many patients relapse due to failed expansion and/or progressive loss of CAR-T cells. We recently reported a strategy to potently restimulate CAR-T cells *in vivo*, enhancing their functionality by administration of a vaccine-like stimulus comprised of surrogate peptide ligands for a CAR linked to a lymph node-targeting amphiphilic PEG-lipid (termed CAR-T-vax). Here, we demonstrate a general strategy to generate and optimize peptide mimotopes enabling CAR-T-vax generation for any CAR. Using the clinical CD19 CAR (FMC63) as a test case, we employed yeast surface display to identify peptide binders to soluble IgG versions of FMC63, which were subsequently affinity matured by directed evolution. CAR-T vaccines using these optimized mimotopes triggered marked expansion and memory development of CD19 CAR-T cells in both syngeneic and humanized mouse models of B-ALL/Lymphoma, and enhanced control of disease progression. This approach thus enables vaccine boosting to be applied to any clinically relevant CAR-T cell product.

Introduction

CD19-targeted chimeric antigen receptor (CAR) T cell therapy elicits impressive anti-tumor activity in the treatment of relapsed or refractory B-cell acute lymphoblastic leukemia (B-ALL) and lymphoma in both pediatric and adult patients[1,2]. This clinical success led to the FDA approval of four CD19-targeted CAR-T products, namely TECARTUS, KYMRIAH, YESCARTA, and BREYANZI[1]. However, a significant fraction (30-60%) of patients still experience leukemia relapse, among which ~50% are CD19-positive relapses[3], suggesting impaired function and/or persistence of the infused CAR-T cells. Robust CAR-T cell engraftment and expansion *in vivo* is a prerequisite for antitumor efficacy[4], a feature that is affected by several characteristics of the CAR-T cell product such as T cell quality[5], CAR designs[3,4,6] and the proportion of early memory T cells in the product[7]. In current CAR-T cell therapy treatment regimens, patients usually receive lymphodepletion to promote CAR-T cell engraftment[8]. Interestingly, multiple reports have shown a correlation between the early-stage expansion of CAR-T cells and initial tumor burden[8,9]. These findings suggest the capacity of CAR-T cells to receive antigen-specific stimulation post-infusion is critical for CAR-T cell expansion, engraftment, and potentially long-term persistence. However, whether the antigens presented by tumor cells are sufficient to optimally stimulate CAR-T cells remains unclear.

Vaccination is a natural process whereby T-cells receive antigen-specific stimulation leading to proliferation, differentiation, and induction of effector functions[10]– effects which could be beneficial in promoting CAR-T cell function *in vivo*. However, traditional vaccines provide antigens that must be processed into peptides by professional antigen-presenting cells (APCs) and presented on the major histocompatibility complex (MHC) molecules to stimulate T-cells through the T-cell receptor (TCR). This is challenging to adapt to the setting of engineered CAR-T cells, as current CAR-T products are polyclonal and express uncharacterized TCRs. Further, recent next-generation engineering efforts such as knocking CARs into the TCR locus produce CAR-T lacking endogenous TCRs[11]. Proof of concept demonstration of CAR-T cells generated from virus-specific T cells followed by vaccine boosting via the viral-specific TCR has been shown in small clinical trials, yet the benefits observed with this approach have been limited[12,13].

To overcome these issues, we recently developed a molecularly-targeted amphiphilic vaccine (amph-vax) approach to directly stimulate CAR-T cells through the chimeric antigen receptor[14,15]. Amph-vax molecules were generated by linking a CAR-ligand to albumin-binding phospholipid polymers. Following parenteral injection, these CAR-ligand conjugates associate with endogenous albumin present in interstitial fluid and are carried into lymph and downstream draining lymph nodes (dLNs). In the dLN, the lipid tails of amph-vax ligands insert into cell membranes, including membranes of professional APCs, allowing APCs to directly “present” the CAR ligand to CAR-T cells together with additional co-stimulation and cytokine support, making them *de novo* CAR-T cell-priming APCs (**Extended Data Fig. 1**)[14]. Amph-vax stimulation led to pronounced CAR-T cell expansion with enhanced functionality, memory formation and substantially enhanced tumor clearance[14,15]. Importantly, we also found that vaccine boosting of CAR-T cells promotes antigen spreading and the induction of endogenous anti-tumor immune responses, which prevent antigen loss-mediated tumor escape[15]. We demonstrated these effects using CARs that recognize synthetic ligands (e.g., fluorescein) and a model EGFRvIII-specific CAR, where the scFv domain of the chimeric receptor recognized a linear peptide epitope in EGFRvIII that is readily synthesized as an amph-ligand. However, to generalize this strategy and enable amph-vax boosting with any arbitrary CAR of interest, an approach is needed for *de novo* generation of surrogate peptide ligands for chimeric antigen receptors.

Here, we demonstrate a workflow to identify peptide mimotope ligands for CAR receptors using yeast surface display-based directed evolution[16], which allows for the generation of amph-vaccines that can be used with any CAR system. We demonstrate the pipeline by discovering an amph-ligand that can be used with all four FDA-approved CD19 CAR-T cell therapies. We created

154 a customized mimotope yeast library to identify peptides that bind to the licensed CD19 CARs.
155 Affinity maturation of hits from this library led to the identification of a peptide with high affinity for
156 the CAR. An amphiphile mimotope (amph-mimotope) vaccine based on this peptide efficiently
157 stimulated CD19 CAR-T cells *in vitro*, triggered their expansion *in vivo*, and enhanced clearance
158 of leukemia in both syngeneic and humanized mouse models of B-ALL/Lymphoma. To show
159 generality, we also generated amph-mimotopes for a second human CAR recognizing the
160 anaplastic lymphoma kinase (ALK) antigen and a murine CD19 CAR. Collectively, these results
161 show the successful development of a clinically translatable amph-mimotope vaccine with the
162 potential for endowing currently FDA-approved CD19 CAR-T cell therapies with enhanced anti-
163 leukemic activity.
164
165 **Results**
166
167 **Antigen$^+$ tumor cells drive transient CD19 CAR-T expansion but are insufficient to promote**
168 **long-term CAR-T persistence**

169 CD19-positive relapse is often associated with limited CAR-T persistence and/or impaired
170 functionality[3,17]. To provide insight into whether the level of available antigen stimulation impacts
171 early CAR-T expansion/persistence, we analyzed data from several early clinical trials in children
172 and young adults (CAYA) with B-ALL from the Children's Hospital of Philadelphia (NCT01626495
173 [18] and NCT02906371[19]) and in adult patients with B-ALL (NCT02030847[20]) or B-cell lymphoma
174 (NCT02030834[21]) from the University of Pennsylvania. We found that CAR-T cell expansion is
175 generally associated with initial tumor burden, with CAR-T cells infused into patients with high
176 tumor burden (>40% bone marrow blasts in pre-infusion bone marrow aspirate) exhibiting more
177 pronounced expansion and longer persistence (**Fig. 1A-C, Extended Data Fig. 2A-B**). This
178 association is statistically significant in CAYA with B-ALL (**Fig. 1A-C**) and exhibits a trend towards
179 significance in adult B-ALL and B-cell lymphoma (**Extended Data Fig. 2A-B**), consistent with
180 observations from earlier studies[8,9].
181 Since CD19 CAR-T cells target normal B cells, continued B cell aplasia can be used as a
182 pharmacodynamic measure for the presence of functional CD19 CAR-T cells[22]. Nearly half of the
183 pediatric B-ALL patients receiving CD19 CAR-T cell therapy experienced B cell recovery after
184 initial B cell aplasia (**Fig. 1D**), indicating loss of functional CAR-T cells. Interestingly, there was
185 no significant association between the initial tumor burden and the probability of B cell recovery,
186 suggesting that increased early stimulation from tumor cells was not sufficient to maintain CAR-T
187 function. A recent long-term follow-up study found that a higher ratio of peak CAR-T expansion to
188 tumor burden correlates with overall survival and is a better prediction of long-term survival than
189 the absolute magnitude of T cell expansion or tumor burden[23]. These data suggest that if CAR-T
190 cells receive greater antigen stimulation following infusion, they can undergo greater expansion,
191 an important correlate of response to therapy[23,24]. However, sustained anti-tumor function over
192 time requires that T-cells receive restimulation by professional APCs, particularly dendritic cells
193 (DCs), which express high levels of costimulatory receptors and cytokines that are lacking from
194 tumor cells and resting B cells[25,26]. By mining a published dataset[27], we observed significantly
195 higher co-stimulatory molecule expression in DCs than healthy and likely-malignant B cells in B-
196 ALL patients (**Fig. 1E, Extended Data Fig. 3A-H**). We previously also observed that the
197 comprehensive suite of costimulatory molecules expressed by DCs is essential for promoting
198 memory differentiation and optimal amplification of CAR-T cells during vaccine boosting[14]. These
199 observations suggested to us that an efficient and safe DC-targeted vaccination approach to
200 reinvigorate and sustain CAR-T cell function could be impactful for enhancing current clinical
201 CD19-targeting CAR-T cell therapies.
202
203 **Discovery of peptide ligands for CARs using yeast surface display**

We previously demonstrated that a CAR-specific amph-vaccine could provide potent stimulation of CAR-T cells *in vivo*[14,15]. The vaccine was created by linking a CAR ligand to an albumin-binding PEG-lipid, which upon co-administration with adjuvant, would efficiently traffic to draining lymph nodes and decorate the surface of APCs, allowing presentation of the ligand to CAR-T cells in the LN (**Extended Data Fig. 1**). We demonstrated this proof of concept using CARs that recognized arbitrary small molecule ligands (e.g., fluorescein (FITC)) or linear peptide epitopes [14]. However, the antibody-based antigen-binding domain of the FDA-approved CD19 CARs (which employ an antibody clone known as FMC63) binds to a conformational epitope spanning multiple domains of the human CD19 antigen[28]. Further, the CD19 extracellular domain (ECD) is difficult to express and prone to misfolding[29], making it challenging to use recombinant CD19 for manufacturing an amphiphile vaccine to stimulate CD19 CAR-T cells. As it is common for CAR binding domains to recognize complex conformational epitopes[30–32], we sought to establish a general strategy to generate simple surrogate ligands for any CAR. We hypothesized that the generation of mimotopes, linear synthetic peptides that are also recognized by the CAR binding domain in addition to its native target antigen, could be an ideal option (**Fig. 2A**).

To identify mimotopes for FMC63, we employed a yeast surface display library[32] presenting ~$5x10^8$ randomized linear peptides of 10 amino acids (AA, 10mer) for screening against recombinant FMC63 expressed as a full-length IgG (hereafter, $FMC63^{IgG}$, **Fig. 2B**). Initial screening was performed using biotinylated $FMC63^{IgG}$ attached to streptavidin beads for magnetic enrichment of weakly-bound yeast clones. After a single round of screening using this enrichment protocol, flow cytometry analysis identified two yeast populations P1 and P2, which bound with higher or lower relative affinity to $FMC63^{IgG}$, respectively, but not an isotype control antibody (**Fig. 2C**). The two peptides shared a common enriched sequence motif RXCPWXCXXX. The presence of two cysteines in the mimotope motif suggested the possibility that these mimotopes formed an intramolecular disulfide bond, with the proline between the two cysteines likely promoting a hairpin formation in the peptide structure[33]. Computational modeling of P1 (RHCPWNCSLL) and P2 (RICPWSCRAP) interactions with FMC63 using AlphaFold predicted the mimotopes take on a curved alpha-helical structure, suggesting the formation of a cyclic structure with an intra-peptide disulfide bond (**Fig. 2D**).

To confirm the presence of a disulfide bond within the mimotope and test whether the disulfide is necessary for peptide binding to $FMC63^{IgG}$, we treated the yeast clone P1 with increasing concentrations of the reducing agent dithiothreitol (DTT, **Fig. 2E**). Treatment with 10 mM DTT lowered Aga2p levels on the yeast cells by ~10-fold, likely due to cleavage of the disulfide linkages anchoring the protein to the yeast cell surface. However, mild reductive conditions (i.e., 0.1mM, 1mM DTT) largely preserved Aga2p on yeast surface but eliminated $FMC63^{IgG}$ binding (**Fig. 2E**). To further verify that this loss in antibody binding reflected loss of a disulfide in the mimotope itself, we chemically synthesized a cyclic version of mimotope P1 and monitored its binding to $FMC63^{IgG}$ using ELISA in the presence or absence of pre-treatment of the peptide with DTT, and found that $FMC63^{IgG}$ recognized plate-bound P1 with an apparent K_D^{IgG} of 1.4 μM, but this binding was completely ablated for DTT-treated P1 (**Fig. 2F**). Next, we created amph-mimotope molecules by conjugating P1 functionalized with an N-terminal azide to DSPE-PEG2k-DBCO through click chemistry (**Fig. 2G**). To test whether the amph-mimotope could insert in cell membranes and enable CD19 CAR-T cell recognition, we labeled CD19-negative K562 cells with amph-P1 and then incubated them with human CD19 CAR-T cells *in vitro* (**Fig. 2G**). Amph-P1-decorated K562 cells effectively triggered IFN-γ secretion from CD19 CAR-T cells but to a much lesser extent than NALM6 cells (**Fig. 2H)**. By contrast, amph-P1 failed to stimulate control EGFRvIII CAR-T cells which responded robustly to amph-pepvIII (pepvIII, a minimal epitope from EGFRvIII, **Fig. 2I**). These results confirmed that P1 is a functional mimotope with a cyclic conformation required for its specific recognition by FMC63.

To demonstrate that the yeast mimotope library is suitable for identifying mimotopes for any desired antibody, we repeated the library screen using an anti-mouse CD19 antibody (Clone

1D3) (**Extended Data Fig. 4A-D**) and an anti-human Anaplastic Lymphoma Kinase (ALK) antibody of interest for CAR-T cell treatment of lymphoma and some lung cancers (**Extended Data Fig. 4E-F**). These additional library screens successfully identified multiple binders for each antibody, highlighting the potential of yeast surface display to effectively identify antibody-specific mimotope peptides.

Affinity maturation of the CD19 mimotope

The affinity of a typical CAR toward its ligand is often in the low nanomolar range[34], however, mimotope P1 only exhibited a low micromolar apparent affinity toward $FMC63^{IgG}$, and this apparent K_D is likely a substantial overestimate of the monovalent affinity of the peptide for FMC63 given the bivalent IgG format used in our binding assays. We therefore aimed to further evolve the mimotope to obtain variants with enhanced affinity. To this end, a new mimotope library V2 was generated bearing a shared motif derived from the two parental mimotopes, namely RXCPWXCXXX, with a diversity of ~1.5×10^8 (**Fig. 3A**). We pre-enriched the V2 mimotope library for binders using $FMC63^{IgG}$-coated magnetic beads (see Materials and Methods)**,** and found that a significant portion of this bead-enriched library V2 could be positively stained with 20 nM biotinylated $FMC63^{IgG}$, while the original P1 yeast clone showed no detectable binding at this concentration (**Fig. 3B**). Flow cytometry sorting of the top 1% of the positive yeast cells followed by sanger sequencing yielded dozens of mimotope clones. Sequence analysis of these mimotopes revealed a consensus sequence with high-affinity binding potential to $FMC63^{IgG}$ (**Fig. 3C**). Several candidate mimotope clones resembling the consensus sequence were validated experimentally, and all of them exhibited stronger binding than the original clone P1 (**Fig. 3D**). We moved forward with mimotope F12 given its highest resemblance to the consensus sequence and highest binding affinity to $FMC63^{IgG}$. This sequence was bound to FMC63 with an apparent $K_D{}^{IgG}$ of 15.6 nM (again, a value likely overestimating the true monovalent K_D due to the avidity effect of the bivalent FMC63 IgG). Alanine scanning across all AA positions in the F12 peptide confirmed the determining role of R at position 1°, C at positions 3° and 7°, P at position 4°, and W at position 5° (**Fig. 3E**). Residues at the remaining AA positions contributed more modestly to the overall affinity. Interestingly, inserting an extra 1-2 alanines between positions 6° and 7° completely disrupted F12 binding to $FMC63^{IgG}$ (**Fig. 3E**), likely through the disruption of the intra-mimotope disulfide bond. Given the labile nature of the disulfide bond in the mimotope, we sought to test if the disulfide bond can be replaced with a structurally similar yet non-reducible thioacetal bond to produce a more stable mimotope (**Extended Data Fig. 5A-B**). Replacing the disulfide bond with a thioacetal bond completely eliminated its binding to $FMC63^{IgG}$, perhaps because the thioacetal bond is 0.9 angstrom (Å) longer than the disulfide bond (**Extended Data Fig. 5C**).

Next, we sought to evaluate the contribution of the flanking sequence to mimotope binding with $FMC63^{IgG}$. A 17 AA linker $(GGGGS)_3AS$ was initially introduced between the 10-mer mimotope and Aga2p during yeast library construction to avoid steric hindrance. We chemically synthesized F12 mimotope variants with increasing length of the upstream linker and performed ELISA to verify $FMC63^{IgG}$ binding. Strikingly, the addition of even a minimal SAS tri-amino acid linker at the N-terminus of the peptide increased binding of F12 to $FMC63^{IgG}$ by a further ~100-fold (**Fig. 3F**). Given these data, we created a third yeast library V3 with ~1×10^8 diversity with 0-6 and 3-10 flanking residues extended from the N- and C-termini of F12, respectively (**Fig. 3G**), aiming to identify mimotope variants with even higher affinity. We performed kinetic sorting by competing off pre-bound biotinylated monovalent $FMC63^{scFv}$ using non-modified bivalent $FMC63^{IgG}$ and were able to identify yeast populations with prolonged retention of biotinylated $FMC63^{scFv}$, indicative of slower off-rates. Characterization of individual clones identified mimotope variants with further increased affinity compared to the parental F12 clone (**Fig. 3H**). Notably, clone F12-A1 exhibited a further ~10-fold increased affinity toward $FMC63^{scFv}$ compared to F12. In the same competition assay as depicted in **Fig. 3G**, $FMC63^{scFv}$ remained bound on F12-A1

305 yeast surface over 24 hours in the presence of excess soluble FMC63^{IgG} but was competed off
306 the parental F12 clone within half an hour (**Fig. 3I**). Finally, we generated amphiphile conjugates
307 of P1, F12 and F12-A1. When presented on the cell surface, these amph-mimotope variants
308 exhibited apparent K_D^{scFv} values of >1μM, 33.6 nM, and 9.9 nM, respectively (**Fig. 3J**). Therefore,
309 these sequential affinity maturation screens effectively enabled the identification of mimotopes
310 with a much-improved affinity for the CAR antibody.
311

312 **Optimized mimotopes bind to FMC63 without compromising its recognition of CD19**

313 To gain a comprehensive view of how the CD19 mimotope interacts with FMC63, we leveraged a
314 recently solved crystal structure of FMC63^{scFv} in complex with CD19 (PDB:7URV)[30] and modeled
315 mimotope binding to FMC63^{scFv}. Both F12 and F12-A1 were modeled using Alphafold[35] and
316 Rosetta[36], and the FMC63^{scFv}-CD19, FMC63^{scFv}-F12, and FMC63^{scFv}-F12A1 binding interfaces
317 were analyzed using PDBePISA[37]. PDBePISA analysis recovered many of the previously defined
318 interactions between FMC63^{scFv} and CD19 through analysis of polarities and bond lengths **(Fig.**
319 **4A),** confirming the validity of PDBePISA in performing interaction interface analysis. Structural
320 modeling of F12 (**Fig. 4B**) or F12-A1 (**Fig. 4C**) interactions with FMC63^{scFv} showed that these
321 mimotopes engage FMC63^{scFv} at the same domain. The key residues on FMC63^{scFv} that are
322 essential for CD19 binding were found to be Y260, Y261, Y70, G263, W212, G262, S214, K69,
323 Y265, and G129 [30]. Of these key residues, both F12 and F12-A1 engage Y260 and S214 **(Fig.**
324 **4D)**. However, only F12-A1 engages G263 (**Fig. 4D**), which likely explains its stronger binding to
325 FMC63^{scFv} than F12.
326 To experimentally assess potential overlaps in the binding interface of FMC63 to CD19 vs.
327 our mimotope peptides, we pre-blocked FMC63^{scFv}, FMC63^{IgG} or an alternative control anti-CD19
328 antibody HIB19^{IgG} with increasing concentrations of mimotopes F12 or F12-A1, and then added
329 the antibodies to CD19$^+$ NALM6 cells (**Fig. 4E**). When FMC63^{scFv} was pre-blocked with F12
330 peptide, binding to NALM6 cells was only compromised when the F12 concentration was 100 μM,
331 and NALM6 binding was nearly unaffected for FMC63^{IgG}. By contrast, F12-A1 abolished
332 FMC63^{scFv} or FMC63^{IgG} binding to CD19 when the mimotope concentrations were greater than 1
333 or 10 μM, respectively, consistent with its higher affinity for FMC63. However, when FMC63 CAR-
334 expressing Jurkat T cells were pre-blocked with increasing concentrations of F12 or F12-A1 and
335 stimulated with NALM6 cells, CD69 induction on Jurkat cells was not affected (**Fig. 4F**). Thus,
336 despite some ability of the mimotopes to interfere with soluble FMC63 binding to CD19$^+$ cells at
337 high concentrations, FMC63-CAR-T cells retained their full potential of recognizing CD19$^+$
338 leukemic cells even in the presence of mimotopes.
339

340 **Amph-mimotope vaccination triggers FMC63-mCAR-T expansion *in vivo***

341 To test if amph-mimotope vaccines could efficiently stimulate human CD19-targeting CAR-T cells
342 in an immunocompetent mouse model *in vivo*, we established a hybrid CAR by fusing the FMC63
343 scFv to murine CAR signaling domains, (FMC63-mCAR, **Fig. 5A**). First, we validated the ability
344 of the amph-mimotope variants to stimulate FMC63-mCAR-T cells. K562 cells were pre-labeled
345 with amph-mimotope variants and co-cultured with FMC63-mCAR-T cells as in **Fig. 2G.** Amph-
346 mimotope-decorated target cells triggered IFN-γ production from the CAR-T cells, with the
347 stimulation efficiency positively correlating with FMC63-mimotope affinity and amph-F12-A1
348 providing the strongest CAR-T activation, comparable to stimulation by NALM6 cells (**Fig. 5B**).
349 To determine if these amph-mimotopes could be effectively presented by DCs *in vivo*, we
350 vaccinated C57BL/6 mice with 10 nmol amph-F12-A1, a dose we previously found to be effective
351 for amph-peptide stimulation of CAR-T cells. We formulated the mimotope with or without cyclic-
352 di-GMP, a STING agonist added as an adjuvant[38]. Following vaccination, we isolated CD11b$^+$
353 myeloid cells and CD11c$^+$ DCs from the draining inguinal lymph nodes and analyzed the presence

354 of surface-displayed amph-peptides using flow cytometry by staining the cells with biotinylated
355 FMC63^{IgG} (**Extended Data Fig. 6A**). Interestingly, high levels of amph-mimotope were detected
356 on APCs for at least 24 hr, but only when amph-mimotope was co-administered with adjuvant
357 (**Fig. 5C**).
358 Next, we labeled FMC63-mCAR-T cells with cell trace violet (CTV) and transferred them
359 into C57BL/6 mice, followed by vaccination with amph-P1, amph-F12, amph-F12-A1 vaccine, or
360 an irrelevant amph-pepvIII as a control and flow cytometry analysis to detect CAR-T cell
361 proliferation (CTV dilution) 2 days later. This functional test of amph-mimotope stimulation
362 revealed a clear hierarchy of mimotope activity *in vivo*, with amph-P1 eliciting no CAR-T cell
363 proliferation, amph-F12 eliciting limited proliferation, and only amph-F12-A1 triggering
364 proliferation of the entire CAR-T population (**Fig. 5D**). These data suggest there is an affinity
365 threshold for mimotope vaccines to effectively stimulate CAR-T cells *in vivo*.
366 Clinical evidence indicates that lack of antigen exposure soon after adoptive transfer may
367 compromise CAR-T engraftment[39]. To test if amph-mimotope vaccine boosting post adoptive cell
368 transfer could promote FMC63-mCAR-T cell expansion and engraftment in the absence of
369 leukemia, naïve CD45.2^{+} C57BL/6 mice received sublethal lymphodepletion followed by
370 intravenous infusion of either CD45.1^{+} FMC63-mCAR-T or control untransduced T cells (**Fig. 5E**).
371 Without additional treatment, peripheral CD45.1^{+} CAR-T cells only occupied <5% of total CD8^{+} T
372 cells by day 4 and decreased to <3% by day 14 (**Fig. 5E**). By contrast, amph-F12-A1 vaccine
373 boosting rapidly amplified CD45.1 CAR-T cells, reaching ~40% of total peripheral CD8^{+} T cells
374 (~500 CAR-T cells per microliter of blood, **Fig. 5E, Extended Data Fig. 6B**) by day 14 after two
375 weekly vaccinations, and then slowly contracting over the next few weeks.
376
377 **Amph-mimotope vaccine boosting of FMC63-mCAR-T in an immunocompetent mouse**
378 **model of B-ALL/Lymphoma**

379 We next sought to evaluate effects of optimized amph-F12-A1 vaccine boosting of FMC63 CAR-
380 T in an immunocompetent mouse model of CD19^{+} hematological malignancy. We transduced
381 Eμ-Myc B-ALL/Lymphoma cells[40] with human CD19 and firefly luciferase. When these
382 hCD19^{+}Luc^{+} Eμ-Myc cells were inoculated into C57BL/6 mice, animals developed aggressive B-
383 ALL/Lymphoma with 100% penetrance and a median survival of 18 days (**Extended Data Fig.**
384 **7A-C**). FMC63^{IgG} showed minimal binding WT B cells expressing mouse CD19, and FMC63-
385 mCAR-T effectively killed hCD19^{+} but not WT Eμ-Myc cells *in vitro* (**Extended Data Fig. 7D-E**).
386 On day 4 post leukemia engraftment, mice were infused with FMC63-mCAR-T alone of CAR-T
387 combined with three weekly amph-mimotope vaccine boosts (**Fig. 6A**). Treatment with CAR-T
388 alone resulted in moderate leukemia control (**Fig. 6A-B**); however, CAR-T in combination with
389 amph-mimotope boosting markedly suppressed disease progression (**Fig. 6A-B**). Enumeration
390 of CAR-T cells in the blood confirmed that vaccine boosting elicited a rapid CAR-T expansion
391 (**Fig. 6C**). Phenotypically, peripheral CAR-T cells from mice receiving vaccination were dominated
392 by an effector population on day 11, but by day 18, nearly 50% of CAR-T cells in vaccinated mice
393 exhibited a central memory phenotype compared to <20% in non-boosted animals (**Fig. 6D-E**).
394 Vaccine-boosted CAR-T cells also possessed significantly higher cytokine polyfunctionality (**Fig.**
395 **6F-G**). As a result, mice receiving both CAR-T and amph-mimotope vaccine had greatly extended
396 survival compared to those receiving CAR-T cells alone (**Fig. 6H**). Lymph nodes of amph-
397 mimotope-boosted animals retained organized T and B cell areas suggesting a lack of overt
398 toxicity of the vaccine boost to draining lymph nodes (**Extended Data Fig. 8A-B**), and no
399 mimotope-specific antibodies were induced (**Extended Data Fig. 8C**). Thus, amph-mimotope
400 boosting of FMC63 CAR-T cells induced multiple favorable effects on CAR-T cell phenotype and
401 increased the anti-tumor efficacy of CAR-T therapy.
402 We previously reported amphiphile-fluorescein (amph-FITC) boosting of CAR-T cells bearing
403 bivalent FITC/tumor antigen-specific CARs[14]. To compare amph-mimotope boosting of the FMC63-

404 mCAR vs. this alternative approach in the hCD19$^+$ Eμ-Myc model, we synthesized a tandem
405 FITC/hCD19-targeted murine CAR construct (i.e., αFITC-FMC63-mCAR), employing the same
406 high-affinity anti-FITC scFv we previously tested. *In vitro*, these dual-CAR T cells effectively
407 recognized and killed hCD19$^+$ Eμ-Myc cells (**Extended Data Fig. 7E**). Treatment of Eμ-Myc
408 tumor-bearing animals with tandem αFITC-FMC63-mCAR-T cells alone elicited similar tumor
409 control as the monovalent FMC63-mCAR-T (**Extended Data Fig. 9A-C,** compare with **Fig. 6A-**
410 **B**). However, while animals receiving treatment with the tandem CAR-T alone did not show signs
411 of toxicity until the tumors progressed, all animals receiving the amph-FITC vaccine boost rapidly
412 developed signs of severe toxicity immediately following the first vaccine boost, including
413 hypothermia and hunched posture, and despite similar early tumor control to the non-boosted
414 tandem CAR group, all animals receiving amph-FITC boosting died by day 20 (**Extended Data**
415 **Fig. 9A-D**). By contrast, mice receiving FMC63-mCAR-T + the amph-mimotope vaccine showed
416 no visible signs of toxicity during the treatment course (**Extended Data Fig. 9D**).
417 As the major difference between the amph-FITC and amph-mimotope vaccines is the
418 affinity of the ligands for the CAR (the 4m5.3 scFv used in the FITC CAR binds to fluorescein with
419 K_D = 270fM[41]), we hypothesized that these disparate outcomes reflect an over-stimulation of the
420 tandem αFITC-FMC63-mCAR T cells, leading to an exacerbation of cytokine release syndrome
421 (CRS) when these cells encounter circulating tumor cells in the B-ALL/Lymphoma model.
422 Comparison of CAR-T cell levels in the blood showed that CAR-T expansion induced by the two
423 vaccines was comparable, suggesting that increased toxicity following FITC boosting could not
424 be attributed simply to the number of CAR-T cells present (**Extended Data Fig. 9E**). However,
425 analysis of serum cytokines at day 6 after the first immunization (or earlier from moribund mice)
426 showed severe CRS in mice receiving amph-FITC vaccine + tandem CAR-T as exemplified by
427 massive elevations of serum IL-6, IL-10, and TNF-α (**Extended Data Fig. 9F**). However, these
428 signature CRS cytokines remained at low levels in mice receiving CAR-T only, or FMC63-mCAR-
429 T plus amph-mimotope vaccination (**Extended Data Fig. 9F**). To assess if this discrepancy was
430 triggered by the differential responses of CAR-T cells towards their respective vaccines, we co-
431 cultured CAR-T cells with the amph-vax-labeled K562 cells *in vitro* and found that amph-FITC
432 triggered much higher levels of IFN-γ and TNF-α secretion by tandem CAR-T cells than the amph-
433 mimotope elicited cytokine secretion from FMC63-mCAR-T cells (**Extended Data Fig. 9G-H**).
434 These results suggest that in the setting of cancers where CAR-T cells encounter a substantial
435 frequency of tumor cells in the blood, high-affinity ligand boosting can exacerbate CRS. This
436 provides an important additional rationale for the mimotope discovery pipeline, where moderate
437 affinity ligands can be readily isolated for any given CAR.
438

439 **Amph-mimotope-labeled DCs enhance human CD19 CAR-T expansion and leukemia**
440 **clearance in a humanized mouse model**

441 Human CAR-T cells are routinely evaluated in immunodeficient NSG mice, but this animal model
442 is problematic for testing lymphatics-mediated amph-vaccine boosting, as these mice have
443 generally defective lymph nodes and lymphatic development due to their lack of native
444 lymphocytes[42]. To overcome this technical hurdle, we devised an alternate strategy to test amph-
445 vaccine boosting of human CAR-T cells. We previously showed that amph-ligand vaccine
446 molecules label lymph node-resident DCs, which are the key APC population mediating the amph-
447 vaccine stimulation[14]. To mimic this process in NSG mice in a human-relevant setting, we
448 differentiated human peripheral blood monocytes into DCs *in vitro* and matured them with
449 lipopolysaccharide (LPS) and IFN-γ (**Fig. 7A**). These matured human monocyte-derived DCs
450 (MoDCs) exhibited significantly increased expression of multiple co-stimulatory molecules,
451 including CD80/86, 41BBL, OX40L, and ICOSL (**Fig. 7A**). Incubation of activated MoDCs with
452 amph-F12-A1 led to robust cell surface labeling with the mimotope (DC-mVax, **Fig. 7B**). DC-
453 mVax efficiently stimulated human CD19 CAR-T cell activation *in vitro* (**Fig. 7C**) but were

refractory to CAR-T cell killing (**Extended Data Fig. 10A**), consistent with our prior observations that DCs were not eliminated during vaccine boosting *in vivo*[14], and work suggesting DCs have mechanisms to resist CTL-mediated killing[43,44]. To determine if DC-mVax could activate and expand human CD19 CAR-T cells *in vivo* in the absence of additional antigen, we infused human CD19 CAR-T cells into non-leukemic NSG mice with or without subsequent *i.v*. infusion of DC-mVax (**Fig. 7D-E**). Mice receiving a single dose of DC-mVax 24 hours post CAR-T infusion exhibited significant expansion of CAR-T cells in the peripheral blood compared to those receiving unmodified DCs, and circulating human CD19 CAR-T cells remained detectable at day 30 (**Fig. 7E**). Notably, the extent of CAR-T cell expansion markedly decreased when DC-mVax was infused 7 days post CAR-T cell transfer, indicating that early antigen exposure plays an important role in promoting CAR-T expansion and engraftment (**Fig. 7E**). Repeated dosing of DC-mVax on day 1 and day 7 days led to a further increase in CAR-T cell expansion (**Fig. 7E**).

To determine if DC-mVax boosting could augment the anti-tumor activity of human CD19 CAR-T cells, we established leukemia in NSG mice by infusing luciferase-expressing NALM6 tumor cells as previously described[45]. Suboptimal doses of CD19 CAR-T cells were administered on day 4 followed 24 hours later by repeated *i.v.* infusions of either unmodified DCs or DC-mVax (**Fig. 7F**). Despite the presence of high levels of target cells, CAR-T cells alone showed poor persistence/expansion compared to CAR-T cells boosted with DC-mVax (**Fig. 7G**). Notably, DC-mVax boosting significantly enhanced CAR-T cytokine polyfunctionality (**Extended Data Fig. 10B-C**) and differentiation toward a central memory phenotype (**Extended Data Fig. 10D-E**). While CAR-T cells alone only slightly delayed tumor expansion and moderately prolonged survival, the addition of the DC-mVax boosting enabled this dose of CAR-T cells to substantially slow tumor growth (**Fig. 7H-I**) and 30% of the animals completely rejected their tumors (**Fig. 7J**). Collectively, these results demonstrated that a suitably affinity-matured amph-mimotope could act as an effective vaccine to promote engraftment, expansion, and reinvigoration of human T cells expressing the CAR currently used in all approved CD19-targeting CAR-T products and enhance their anti-leukemic activity.

Discussion

Successful engraftment and persistence is critical for ensuring robust and long-term anti-leukemic activity by CAR-T cells[1,46]. Analysis of data from recent CAR-T cell clinical trials suggested that CD19-directed CAR-T cells initially expand more strongly if there is a high tumor burden, consistent with the idea of CAR-T expansion that is commensurate with the dose of antigen encountered. However, the long-term persistence of CAR-T cells does not correlate with the initial tumor burden, suggesting that this initial stimulus vanishes over time as leukemic cells are cleared from the body and/or that stimulation received from tumor cells or naïve B cells lacking appropriate costimulatory signals is insufficient to maintain the CAR-T cell population. We and others have recently demonstrated the ability of using a synthetic vaccine to boost CAR-T cells *in vivo* and achieved enhanced therapeutic outcomes[14,15,47]. Our strategy of linking a ligand for the CAR to a lymph node-targeting PEG-lipid amphiphile is simple but requires a suitable peptide or protein ligand. The poor expression and misfolding of recombinant human CD19 ectodomain[29] make the use of the native target antigen challenging for this approach. Here we demonstrate that surrogate CAR ligands based on short peptides can be readily identified and affinity-matured using directed evolution, enabling the generation of mimotope vaccines that efficiently boost CD19 CAR-T cells analogous to natural CD19 antigen exposure. Vaccine boosting significantly impacted the outcome of CD19 CAR-T cell therapy by increasing CAR-T cell expansion and engraftment as well as augmenting CAR-T cell functionality. Importantly, the mimotope vaccine discovered here is applicable to all four FDA-approved FMC63-based CD19 CAR-T cell therapies.

In addition to the human CD19 CAR mimotope, mimotopes for anti-mouse CD19 and anti-human ALK CARs were also successfully identified using the same yeast mimotope library,

504 indicating the broad applicability of this library for identifying mimotopes for any desired antibody.
505 Experimental verification and structural modeling demonstrated that the CD19 mimotope
506 discovered through the yeast library forms a cyclic conformation that is essential for its recognition
507 by FMC63. Given that FMC63 recognizes a conformational epitope, it is possible that a mimotope
508 also needs to form a desired secondary structure to achieve strong binding. Notably, the CD19
509 mimotope only partially occupies the natural epitope binding domain on FMC63. This partial
510 occupancy appears to enable FMC63-based CD19 CAR-T cells to maintain their capacity to
511 recognize $CD19^+$ leukemia cells even in the presence of the mimotope, which could be important
512 for allowing the CAR-T cells to continue sensing tumor cells in lymph nodes during vaccine
513 boosting. The transient surface presentation of amph-ligands also prevents CAR-T cells from
514 receiving excessive and prolonged antigen exposure, thus reducing the likelihood of CAR-T cell
515 exhaustion and severe cytokine release syndrome[14].
516 We previously reported an alternative approach for vaccine boosting CAR-T, where the
517 CAR itself is engineered as a tandem CAR with one binding domain recognizing a tumor antigen
518 and the other domain binding to the synthetic molecule FITC, enabling boosting of these tandem
519 CARs with the amph-FITC vaccine[14,15]. While this approach avoids the need to generate a new
520 amph-vaccine for each new CAR product, many CARs (such as the FMC63-based CAR products)
521 have already reached extensive clinical testing, providing a strong motivation to leave the CAR
522 design itself unchanged. In addition, the tendency of scFvs to undergo aggregation that can
523 induce detrimental tonic signaling in CAR T cells[48–50] may make the bivalent CAR approach
524 untenable for some CARs. In these settings, the amph-mimotope strategy is an ideal solution.
525 While B cells retain the antigen for CAR-T, evidence suggests that B cells themselves may
526 not be as effective as conventional DCs for restimulating CAR-T cells at least partially due to
527 greater expression of co-stimulatory molecules in DCs[26]. Our previous findings showed that co-
528 stimulatory molecules expressed by activated DCs are crucial for optimally expanding CAR-T
529 cells with amph-ligands[14]. This DC-specific effect is further exemplified in our DC-mVax boosting
530 of human CAR-T in NSG mice and amph-mimotope vaccine boosting of mouse CAR-T in the Eμ-
531 Myc B-ALL/Lymphoma mouse model, where vaccination not only drove CAR-T expansion but
532 also enhanced effector cytokine expression and promoted memory differentiation. Conventional
533 CD19 CAR-T cells expand and show efficacy following the first infusion, however, reinfusion of
534 CAR-T cells into patients experiencing $CD19^+$ tumor relapse is often ineffective, with significantly
535 lower CAR-T expansion compared to the first infusion[39,51–53]. Therefore, one potential use of the
536 mimotope vaccine is to support CAR-T cells during reinfusion. Notably, even during the first
537 infusion, CD19 CAR-T cells rapidly decline after a transient expansion[9,54]. Despite the general
538 correlation of initial CAR-T expansion with baseline tumor burden, a long-term follow-up study in
539 B-ALL found that a higher ratio of peak CAR-T-cell expansion to tumor burden significantly
540 correlated with event-free survival and overall survival[23]. Although this effective ratio more likely
541 occurs in patients with lower tumor burden, administering the mimotope vaccine upon CAR-T
542 contraction during the first infusion could potentially reinvigorate CAR-T cells and sustain CAR-T
543 expansion to elevate this effective ratio in patients with both low and high tumor burden to improve
544 event-free survival.
545 Given the toxicity associated with rapid CAR-T activation and expansion in patients with
546 hematological malignancies, such as CRS and immune effector cell-associated neurotoxicity
547 syndrome (ICANS), amph-vaccine affinity, dose, and dosing intervals may need to be tailored
548 based on the CAR-T cell number and residual tumor burden in patients in future clinical trials. In
549 our previous work, the amph-FITC vax/tandem CAR-T combination enhanced CAR-T therapy
550 against solid tumors with transient mild toxicity[14]. However, in a side-by-side comparison, we
551 found that the amph-FITC vax/tandem CAR-T combination triggered a lethal CRS in the
552 immunocompetent Eμ-Myc B-ALL/Lymphoma mouse model, while amph-mimotope vax/CAR-T
553 treatment effectively controlled leukemia progression with limited toxicity. Our data suggests this
554 drastic discrepancy in toxicity profiles is linked to the much higher affinity of the tandem CAR

towards the amph-FITC vaccine vs. the amph-mimotope binding to FMC63. These data indicate that amph-vaccine ligand affinity plays a critical role in the outcome of CAR-T boosting in cancers involving substantial levels of circulating tumor cells that will trigger cytokine secretion in the blood. The mimotope discovery pipeline described here is well suited to identify effective and safe ligands, as it allows mimotopes with a wide range of affinities to be discovered.

One set of challenges for characterizing amph-vaccines designed for human T cells are the deficiencies of current humanized mouse models. The defective lymphatics, absent or disorganized lymph nodes, and poor crosstalk of mouse APCs with human T cells is a barrier to evaluating vaccine boosting of human CAR-T cells in NSG mice[42]. As an alternative, we evaluated vaccine boosting of mouse T cells bearing a hybrid FMC63-mCAR in immunocompetent C57BL/6 mice via standard vaccine administration routes and boosting of human CD19 CAR-T cells using mimotope-decorated human MoDCs in NSG mice via *i.v.* delivery. These two complementary approaches demonstrated the feasibility of the mimotope vaccine in the setting of natural trafficking and distribution from lymphatics to lymph nodes, as well as its capacity to stimulate human CAR-T cells upon insertion into the surface of human DCs.

mRNA vaccines encoding the target tumor antigen can also be employed to stimulate CAR-T cells[47]. Recently, a CLDN6-expressing mRNA vaccine was tested in a phase 1 clinical trial in combination with CLDN6-directed CAR-T cells and showed promise in improving CAR-T cell expansion in patients with solid tumors[55]. Importantly, CAR-T plus mRNA vaccination was well tolerated, suggesting the overall safety profile associated with this combination therapy. However, mRNA-LNPs differ from our amphiphile vaccines in their *in vivo* trafficking, biodistribution, and the duration of antigen presentation on the cell surface. Therefore their differential effects on boosting human CD19 CAR-T cells remain to be determined.

In summary, we have designed and validated a general strategy to generate mimotope ligands for any CAR. Using this methodology, we demonstrate an amph-mimotope vaccine that could be used clinically in tandem with all four FDA-approved CD19 CAR-T cell products. The ability of amph-mimotope vaccines to efficiently stimulate human CD19 CAR-T cells *in vivo* supports its potential use as a robust and clinically translatable approach for enhancing the engraftment, long-term persistence, and anti-leukemic activity of current CD19 CAR-T cell therapies.

ACKNOWLEDGMENTS

We thank the Koch Institute Swanson Biotechnology Center for technical support, specifically the flow cytometry core facility. We thank Dr. Michael Hemann from the Koch Institute of MIT for sharing the Eμ-Myc cells. We thank Dr. Steve Albelda for his suggestions on the manuscript. **Funding:** This work was supported by the NIH (award EB022433 to DJI), the Marble Center for Nanomedicine (to DJI), and the Mark Foundation for Cancer Research (to DJI). L.M was supported by an American Cancer Society postdoctoral fellowship, the Cell and Gene Therapy Collaborative and the Junior faculty pilot program at CHOP, NIH New Innovators Award (DP2 AI164319-03), ITMAT at UPenn and NCATS (UL1TR001878). This work is also partially supported by Cancer Center Support (core) Grant P30-CA14051 from the NCI to the Barbara K. Ostrom (1978) Bioinformatics and Computing Core Facility of the Swanson Biotechnology Center. D.J.I. is an investigator of the Howard Hughes Medical Institute. R.R. and A.N are supported by a National Science Foundation Graduate Research Fellowship Program award. Parisa Yousefpour is supported by an NRSA F32 fellowship (award AI164829) from the NIH. M.R. is supported by the NIH NCI P01 PCA214278C, the R01/37-CA262362-01A1, the Laffey McHugh Foundation, and the Berman and Maguire Funds for Lymphoma Research at Penn. G.G is supported by the SITC-Mallinckrodt Pharmaceuticals Adverse Events in Cancer Immunotherapy Clinical Fellowship, and the Mario Luvini fellowship grant—Fondazione Ticinese per la Ricerca sul Cancro.

Data and materials availability: All data are available on request.

AUTHOR CONTRIBUTIONS

L.M., D.J.I., and K.D.W designed the studies. L.M., T.M.G., R.R., and D.J.I. analyzed and interpreted the data and wrote the manuscript. L.M and N.M generated yeast mimotope libraries. L.M. and T.M.G performed the experiments. B.C and I.S assisted with mimotope identification. D.M.M. mined single cell RNA-sequencing data. L.M., L.Z., and R.S. carried out amphiphile-mimotope synthesis. R.R. performed structural modeling. I.S. P.Y. and H.S. assisted with sample preparation. W.A., A.N., R.T., and A.C. assisted with animal experiments. A.R. performed lymph nodes immunofluorescence studies. B.G. performed ELISA analysis. S.K., R.M.M., S.A.G., L.P., G.G., S.J.S, N.F. and M.R. processed and provided the clinical data. E.B. and R.C assisted with ALK mimotope identification and verification.

DECLARATION OF INTERESTS

L.M and D.J.I are inventors on patents filed related to the amphiphile-mimotope vaccine technology. G.G. served as a scientific consultant for viTToria Biotherapeutics. M.R. holds patents related to CD19 CAR-T cells, served as a consultant for NanoString, Bristol Myers Squibb,GlaxoSmithKline, Scaylite, Bayer, and AbClon, receives research funding from AbClon,NanoString, Oxford NanoImaging, viTToria biotherapeutics, CURIOX, and Beckman Coulter. M.R. is the scientific founder of viTToria Biotherapeutics

656
657 **FIGURE LEGENDS**
658
659 **Figure 1: CD19 CAR-T cell expansion and B cell aplasia in pediatric B-ALL patients with**
660 **initial high or low tumor burden, and rationale for a DC-targeting CD19-CAR stimulating**
661 **vaccine**. (**A**) Scatterplot of peripherally circulating CAR-T cells in pediatric B-ALL patients with
662 initially high (≥40%, *n*=40) or low tumor burden (<40%, *n*=90) measured by quantitative
663 polymerase chain reaction (qPCR) over time during the first month after infusion. Solid lines show
664 trends generated by locally estimated scatterplot smoothing (loess). The median time to peak
665 CAR-T expansion was 10 days after infusion in both cohorts. (**B**) Maximum concentration and (**C**)
666 Area under the curve (AUC) of CAR-Transgene levels measured by qPCR, broken down by tumor
667 burden. ***, p<0.001, by Wilcoxon rank-sum tests. (**D**) Kaplan-Meier analysis of B cell aplasia for
668 all patients (black) or high (orange) or low (blue) tumor burden patients. B cell aplasia is defined
669 as the time to the emergence of ≥1% CD19-positive B cell in bone marrow aspirate or ≥3% B cell
670 by peripheral blood flow cytometry or CD19-positive relapse. Data were censored for patients
671 who had CD19-negative relapse, reinfusion for hematogones in the marrow, alternative therapy
672 including other CAR-T therapy or hematopoietic stem cell transplant, or non-relapse mortality. The
673 probability of continued B-cell aplasia at two years was similar in both cohorts (p = 0.76). At 6
674 months, it was 72% (95% CI 55-95) in high and 67% (95% CI 57-78) in low tumor burden patients.
675 (**E**) Box plot of costimulatory molecule module scores expressed by B cells (likely-healthy and
676 likely-malignant) and DC. Each point represents the average of all cells of that phenotype within
677 a patient. ****, p<0.0001, by a two-sided Wilcoxon rank-sum test.
678
679 **Figure 2: Yeast surface display identifies CD19-CAR binding mimotopes.** (**A**) Illustration of
680 CD19-CAR stimulation by natural CD19 or amph-mimotope. (**B**) Yeast surface display workflow
681 for identifying antibody-specific mimotopes. (**C**) Flow cytometry plots showing the successful
682 identification of yeast cell populations (P1 and P2) binding to 1 μM $FMC63^{IgG}$ after a single round
683 of magnetic enrichment. (**D**) Structural modeling of mimotopes P1 and P2 binding to FMC63. (**E**)
684 Impact of the disulfide bond on mimotope binding to $FMC63^{IgG}$ on yeast surface. Yeast cells
685 bearing mimotope P1 were treated with increasing concentrations of DTT, and then stained with
686 500 nM biotin-$FMC63^{IgG}$ and an anti-HA tag antibody for analysis of binding by flow cytometry. (**F**)
687 ELISA analysis showing the impact of the disulfide bond on synthetic mimotope binding to
688 $FMC63^{IgG}$. (**G**) Scheme for amph-mimotope generation by click chemistry linkage of azide-
689 modified P1 to DBCO-PEG-DSPE, and schematic illustration of amph-P1 coating of target cells.
690 (**H**) $CD19^{-}$ K562 cells labeled with 100 nM amph-P1, unlabled K562 cells, or $CD19^{+}$ NALM6 cells
691 were co-cultured with CD19 CAR-T at a 5:1 E:T ratio for 6 hr followed by IFN-γ ELISA. (**I**) K562
692 cells unlabeled, labeled with 100 nM amph-P1, or labeled with 100 nM amph-pepvIII were co-
693 cultured with control EGFRvIII-CAR-T cells at a 5:1 E:T ratio for 6 hours followed by IFN-γ ELISA.
694 Error bars show mean ± s.d. with triplicate samples. **, p<0.01 by one-way ANOVA with Turkey's
695 post-test. A, B, and G are created with BioRender.com.
696
697 **Figure 3: Affinity maturation of CD19 mimotopes.** (**A**) Schematic workflow for identifying
698 affinity-enhanced mimotope variants of P1 from a motif-fixed mimotope library V2. Created with
699 BioRender.com. (**B**) Flow cytometry plots of 20 nM $FMC63^{IgG}$ binding to yeast cells expressing
700 the V2 mimotope library. The yeast clone P1 was included as a control. The V2 mimotope library
701 was pre-enriched using $FMC63^{IgG}$-coated magnetic beads (see materials and methods). (**C**)
702 Weblogo showing the consensus mimotope sequence with high-affinity binding to $FMC63^{IgG}$. (**D**)
703 Binding of $FMC63^{IgG}$ to select yeast clones assessed by flow cytometry. Amino acid sequences
704 and apparent binding affinity are shown for each yeast clone. Median fluorescence intensities
705 (MFI) at each concentration were fit for the calculation of apparent K_Ds . (**E**) Impact of individual
706 AA positions on $FMC63^{IgG}$ binding. Yeast clones bearing F12 variants with 1-2 alanine (Red)

707 insertions or individual AA mutated to alanine (Red) were assessed for FMC63^{IgG} binding by flow
708 cytometry. (**F**) ELISA showing the impact of flanking residues on mimotope^{F12} binding to FMC63^{IgG}.
709 The apparent binding affinity was determined as in D. (**G**) Schematic workflow for identifying
710 affinity-enhanced mimotopes from mimotope library V3 using kinetic sorting. Yeast library V3 was
711 first stained with monovalent biotin-FMC63scFv, followed by competition with non-biotinylated
712 bivalent FMC63^{IgG}. Created with BioRender.com. (**H**) Binding of FMC63^{scFv} to select yeast clones
713 bearing various evolved mimotopes. The parental mimotope^{F12} sequence was underlined. The
714 apparent binding affinity was determined as in D and specified after the mimotope sequence. (**I**)
715 Representative histograms showing retention of prebound FMC63^{scFv} on yeast clone F12-A1 in
716 the presence of FMC63^{IgG}. Yeast cells were pre-stained with 50nM Biotin-FMC63^{scFv} followed by
717 incubation with 1μM FMC63^{IgG}. Yeast cells were sampled at indicated times for PE-streptavidin
718 staining as an indicator for the retention of Biotin-FMC63^{scFv}. (**J**) CD19^{-} K562 cells were labeled
719 by incubation with 500 nM of the indicated amph-mimotopes, washed, then incubated with various
720 concentrations of fluorescent FMC63^{scFv} followed by flow cytometry analysis of scFv binding;
721 apparent binding affinities were determined as in **H**. Error bars show mean ± s.d. with triplicate
722 samples.
723
724
725 **Figure 4: Structural modeling of mimotopes complexed with FMC63. (A)** Ribbon diagram of
726 FMC63^{scFv} (purple) in complex with human CD19 (green, PDB 7URV). Interactions involving key
727 residues of FMC63 are shown. Interacting sidechain atoms are shown and boxed. Interactions
728 involving backbone atoms are labeled without box. **(B-C)** Computational models generated using
729 Alphafold and Rosetta for FMC63^{scFv} bound to F12 (**B**) or F12-A1 (**C**), respectively. Interactions
730 involving previously mentioned key residues of FMC63 are labeled using the same scheme as in
731 A. For F12-A1, the orientation of mimotope is shown to best exhibit how it engages FMC63. The
732 panel in the bottom left depicts the complex in the same orientation as F12-FMC63. **(D)** Interface
733 footprint of mimotopes on FMC63. On the left side, the CD19 interface is shown in green, the F12
734 interface shown in orange, and overlapping residues are shown in red. On the right side, the CD19
735 interface is shown in green, the F12A1 interface shown in blue, and overlapping are residues
736 shown in red. **(E)** Recognition of natural CD19 recognition by FMC63^{scFv} in the presence of
737 mimotopes. Biotinylated FMC63^{scFv} was pre-incubated with various concentrations of F12 or F12-
738 A1 prior to staining NALM6 cells and detection via PE-conjugated streptavidin. For FMC63^{IgG}
739 binding, NALM6 cells were stained with the same concentrations of mimotope and FMC63^{IgG} with
740 no prior incubation, and binding was detected using PE-conjugated anti-mouse-IgG. A non-
741 competing IgG clone HIB19 is shown as a control. **(F)** Activation of mimotope-bound CD19 CAR-
742 T cells by target cells. CD19-CAR Jurkat T cells were pre-incubated with F12 or F12-A1 at
743 indicated concentrations, then co-cultured with NALM6 cells at a 1:1 E:T ratio for 16 hours
744 followed by flow cytometry analysis of CD69 expression. Shown in E-F are one representative
745 results of three independent experiments.
746
747 **Figure 5: Amph-mimotopes require a threshold affinity to stimulate CAR-T proliferation in**
748 **vivo**. (**A**) Schematic of hybrid FMC63-mCAR design. (**B**) Comparison with various amph-
749 mimotopes in stimulating FMC63-mCAR-T cells. K562 cells were labeled with 100 nM of amph-
750 mimotope variants for 30 min, washed, and co-cultured with FMC63-mCAR-T cells at a 1:1 E:T
751 ratio for 6 hours followed by ELISA measurement of IFN-γ secretion. (**C**) Amph-mimotope labeling
752 of APCs *in vivo*. C57BL/6 mice (*n*=3 animals/group) were vaccinated with 10 nmol amph-
753 mimotope ± CDG adjuvant, and 24 or 48 hr later, mimotope uptake by macrophages and cDCs
754 was detected by staining with FMC63 followed by flow cytometry analysis. Shown are
755 representative histograms of FMC63 staining. (**D**) Amph-mimotope vaccine stimulation of CAR-T

cells *in vivo*. WT C57BL/6 mice (*n*=3 animals/group) received adoptively transferred with $2x10^6$ CTV-labeled FMC63-mCAR-T cells, then vaccinated 1 day later with 10 nmol amph-peptides + 25µg CDG adjuvant (Vax). Shown above is the timeline and below are representative histograms of FMC63-mCAR-T cell proliferation in LNs 48 hours after vaccination. (**E**) Longitudinal monitoring of CAR-T expansion in response to amph-mimotope vaccination. C57BL/6 mice (*n*=5 animals/group) were lymphodepleted (L.D.), adoptively transferred with 10^6 FMC63 CAR-T cells, and then vaccinated at indicated time points, and circulating FMC63-mCAR-T cells were quantified in the blood by flow cytometry over time. Error bars show mean ± s.d. with triplicate samples for B, mean ± 95% CI for C-E. ***, p<0.0001;**, p<0.01; n.s., not significant, by one-way ANOVA with Turkey's post-test for B-D, two-way ANOVA with Tukey's post-test for E.

Figure 6: Amph-mimotope vaccine enhances FMC63-mCAR-T therapy in an immunocompetent hCD19$^+$ Eµ-Myc B-ALL/Lymphoma mouse model. (**A-B**) Real-time whole animal imaging tracking disease progression. C57BL/6 albino mice were lymphodepleted (L.D.) and injected with $0.5x10^6$ hCD19$^+$ Luc$^+$ Eµ-Myc cells. On day 4, mice were adoptively transferred with $2x10^6$ FMC63-mCAR-T cells, then vaccinated 1 day later with 10 µg amph-F12-A1 + 25 µg CDG(*n*=8 animals/group). Shown are whole animal imaging at indicated times (**A**), and quantification of total photon counts over time in each group (**B**). (**C**) Enumeration of circulating CAR-T cells or control T cells by flow cytometry over time. (**D-E**) Immunophenotype of circulating CAR-T cells on days 11 and 18. Shown are the representative flow cytometry plots (**D**), and percentages of effector/effector memory (EM, CD44$^+$CD62L$^-$) and central memory (CM, CD44$^+$CD62L$^+$) CAR-T cells (**E**). (**F-G**) Cytokine polyfunctionality of circulating CAR-T cells on day 11. Shown are representative contour plots (**F**), and percentages of cytokine-secreting CAR T cells (**F**). (**H)** The overall survival of Eµ-Myc mice under various treatment regimens. Error bars show mean± 95%CI. *, p=0.0100; **, p<0.01; ***, p<0.001, ****, p<0.0001, by two-way ANOVA with Tukey's post-test for B, by one-way ANOVA with Tukey's post-test for C, by unpaired t-test for E, G, by Log-rank (Mantel-Cox) test for H.

Figure 7: Amph-mimotope vaccine-labeled DCs augment human CD19 CAR-T therapy against leukemia. (**A**) Schematic of approach to generate "DC-mVax" and representative histograms depicting LPS/IFN-γ-induced upregulation of co-stimulatory markers on mature DCs. (**B**) Representative histogram showing FMC63^{IgG} binding to DC-mVax. Activated MoDCs were incubated with 500 nM amph-F12-A1 or control amph-pepvIII for 30min, washed, and then stained with FMC63^{IgG}. (**C**) CAR-T activation by DC-mVax. Activated MoDCs were labeled with amph-F12-A1 or amph-pepvIII as in (**B**) and then co-cultured human CD19 CAR-T cells at a 1:1 E:T ratio. Shown is IFN-γ measured in the supernatant after 6 hr by ELISA. (**D**) Experimental setup and timeline for E. (**E**) Quantification of circulating human CD19 CAR-T cells in the absence or presence of a single dose of DC-mVax at day 1 or day 7 or two weekly doses of DC-mVax administered following timeline in D (n=5 animals/group). (**F**) Experimental setup and timeline for G-J. (**G-J**) Real-time whole animal imaging of B-ALL progression in NSG mice. Human CD19-CAR-T cells were administered with or without DC-mVax and tumor progression was monitored using *in vivo* bioluminescent imaging (*n*=5 animals/group. Shown are the enumeration of circulating human CD19 CAR-T cells on day 21 (**G**), whole animal imaging at indicated times (**H**) and quantification of total photon counts over time (**I**). Shown is one of two independent experiments. (**J**) Overall survival of NSG mice under various treatment regimens. *n*=10 animals assembled from two independent experiments. Shown are combined data from two independent experiments. Error bars show mean ± s.d. with triplicate samples for C, and mean ± 95% CI for E,G, I-J . ***, p<0.0001; **, p<0.01 by Student's t-test for C and G, by two-way ANOVA with Tukey's post-test for E and I, and by Log-rank (Mantel-Cox) test for J.

807
808 **References**
809

810 1. Cappell, K. M. & Kochenderfer, J. N. Long-term outcomes following CAR T cell therapy: what
811 we know so far. *Nat. Rev. Clin. Oncol.* **20**, 359–371 (2023).
812 2. Irvine, D. J., Maus, M. V., Mooney, D. J. & Wong, W. W. The future of engineered immune cell
813 therapies. *Science* **378**, 853–858 (2022).
814 3. Labanieh, L. & Mackall, C. L. CAR immune cells: design principles, resistance and the next
815 generation. *Nature* **614**, 635–648 (2023).
816 4. Bai, Z. *et al.* Single-cell antigen-specific landscape of CAR T infusion product identifies
817 determinants of CD19-positive relapse in patients with ALL. *Sci. Adv.* **8**, eabj2820 (2022).
818 5. Wang, X. & Rivière, I. Clinical manufacturing of CAR T cells: foundation of a promising therapy.
819 *Mol. Ther. - Oncolytics* **3**, 16015 (2016).
820 6. Neeser, A., Ramasubramanian, R., Wang, C. & Ma, L. Engineering enhanced chimeric antigen
821 receptor-T cell therapy for solid tumors. *Immuno-Oncol. Technol.* **19**, 100385 (2023).
822 7. Garfall, A. L. *et al.* T-cell phenotypes associated with effective CAR T-cell therapy in
823 postinduction vs relapsed multiple myeloma. *Blood Adv.* **3**, 2812–2815 (2019).
824 8. Turtle, C. J. *et al.* CD19 CAR–T cells of defined CD4+:CD8+ composition in adult B cell ALL
825 patients. *Journal of Clinical Investigation* **126**, 2123–2138 (2016).
826 9. Kadauke, S. *et al.* Risk-Adapted Preemptive Tocilizumab to Prevent Severe Cytokine Release
827 Syndrome After CTL019 for Pediatric B-Cell Acute Lymphoblastic Leukemia: A Prospective
828 Clinical Trial. *J. Clin. Oncol.* **39**, 920–930 (2021).
829 10. Seder, R. A., Darrah, P. A. & Roederer, M. T-cell quality in memory and protection:
830 implications for vaccine design. *Nat. Rev. Immunol.* **8**, 247–258 (2008).
831 11. Eyquem, J. *et al.* Targeting a CAR to the TRAC locus with CRISPR/Cas9 enhances tumour
832 rejection. *Nature* **543**, 113–117 (2017).
833 12. Rossig, C. *et al.* Vaccination to improve the persistence of CD19CAR gene-modified T cells
834 in relapsed pediatric acute lymphoblastic leukemia. **31**, 1087–1095 (2017).
835 13. Akahori, Y. *et al.* Antitumor activity of CAR-T cells targeting the intracellular oncoprotein WT1
836 can be enhanced by vaccination. *Blood* **132**, 1134–1145 (2018).
837 14. Ma, L. *et al.* Enhanced CAR–T cell activity against solid tumors by vaccine boosting through
838 the chimeric receptor. *Science* **365**, 162–168 (2019).
839 15. Ma, L. *et al.* Vaccine-boosted CAR T crosstalk with host immunity to reject tumors with antigen
840 heterogeneity. *Cell* **186**, 3148-3165.e20 (2023).
841 16. Boder, E. T. & Wittrup, K. D. Yeast surface display for screening combinatorial polypeptide
842 libraries. *Nat. Biotechnol.* **15**, 553–557 (1997).
843 17. Rafiq, S., Hackett, C. S. & Brentjens, R. J. Engineering strategies to overcome the current
844 roadblocks in CAR T cell therapy. *Nat. Rev. Clin. Oncol.* **17**, 147–167 (2020).
845 18. Maude, S. L. *et al.* Chimeric antigen receptor T cells for sustained remissions in leukemia.
846 *New Engl J Medicine* **371**, 1507–17 (2014).
847 19. Kadauke, S. *et al.* Risk-Adapted Preemptive Tocilizumab to Prevent Severe Cytokine Release
848 Syndrome After CTL019 for Pediatric B-Cell Acute Lymphoblastic Leukemia: A Prospective
849 Clinical Trial. *J Clin Oncol* JCO.20.02477 (2021) doi:10.1200/jco.20.02477.
850 20. Frey, N. V. *et al.* Optimizing Chimeric Antigen Receptor T-Cell Therapy for Adults With Acute
851 Lymphoblastic Leukemia. *J. Clin. Oncol. : Off. J. Am. Soc. Clin. Oncol.* **38**, 415–422 (2019).
852 21. J., S. S. *et al.* Chimeric Antigen Receptor T Cells in Refractory B-Cell Lymphomas. *N. Engl.*
853 *J. Med.* **377**, 2545–2554 (2017).
854 22. Maude, S. L. *et al.* Chimeric Antigen Receptor T Cells for Sustained Remissions in Leukemia.
855 *New England Journal of Medicine* **371**, 1507–1517 (2014).
856 23. Park, J. H. *et al.* Long-Term Follow-up of CD19 CAR Therapy in Acute Lymphoblastic
857 Leukemia. *N. Engl. J. Med.* **378**, 449–459 (2018).

24. Fischer, L. *et al.* Cellular dynamics following CAR T cell therapy are associated with response and toxicity in relapsed/refractory myeloma. *Leukemia* 1–11 (2024) doi:10.1038/s41375-023-02129-y.
25. Ho, W. Y., Cooke, M. P., Goodnow, C. C. & Davis, M. M. Resting and anergic B cells are defective in CD28-dependent costimulation of naive CD4+ T cells. *J. Exp. Med.* **179**, 1539–1549 (1994).
26. Lim, T. S. *et al.* CD80 and CD86 Differentially Regulate Mechanical Interactions of T-Cells with Antigen-Presenting Dendritic Cells and B-Cells. *PLoS ONE* **7**, e45185 (2012).
27. Witkowski, M. T. *et al.* Extensive Remodeling of the Immune Microenvironment in B Cell Acute Lymphoblastic Leukemia. *Cancer Cell* **37**, 867-882.e12 (2020).
28. Klesmith, J. R., Wu, L., Lobb, R. R., Rennert, P. D. & Hackel, B. J. Fine Epitope Mapping of the CD19 Extracellular Domain Promotes Design. *Biochemistry* **58**, 4869–4881 (2019).
29. Laurent, E. *et al.* Directed Evolution of Stabilized Monomeric CD19 for Monovalent CAR Interaction Studies and Monitoring of CAR-T Cell Patients. *ACS Synth. Biol.* **10**, 1184–1198 (2021).
30. He, C. *et al.* CD19 CAR antigen engagement mechanisms and affinity tuning. *Sci. Immunol.* **8**, eadf1426 (2023).
31. Li, N. *et al.* CAR T cells targeting tumor-associated exons of glypican 2 regress neuroblastoma in mice. *Cell Rep. Med.* **2**, 100297 (2021).
32. Wellhausen, N. *et al.* Epitope base editing CD45 in hematopoietic cells enables universal blood cancer immune therapy. *Sci. Transl. Med.* **15**, eadi1145 (2023).
33. Melnikov, S. *et al.* Molecular insights into protein synthesis with proline residues. *EMBO Rep.* **17**, 1776–1784 (2016).
34. Foote, J. & Eisen, H. N. Breaking the affinity ceiling for antibodies and T cell receptors. *Proc. Natl. Acad. Sci.* **97**, 10679–10681 (2000).
35. Jumper, J. *et al.* Highly accurate protein structure prediction with AlphaFold. *Nature* **596**, 583–589 (2021).
36. Rohl, C. A., Strauss, C. E. M., Misura, K. M. S. & Baker, D. Protein Structure Prediction Using Rosetta. *Methods Enzym.* **383**, 66–93 (2004).
37. Krissinel, E. & Henrick, K. Inference of Macromolecular Assemblies from Crystalline State. *J. Mol. Biol.* **372**, 774–797 (2007).
38. Burdette, D. L. *et al.* STING is a direct innate immune sensor of cyclic-di-GMP. *Nature* **478**, 515–518 (2011).
39. Holland, E. M. *et al.* Efficacy of second CAR-T (CART2) infusion limited by poor CART expansion and antigen modulation. *J. Immunother. Cancer* **10**, e004483 (2022).
40. Adams, J. M. *et al.* The c-myc oncogene driven by immunoglobulin enhancers induces lymphoid malignancy in transgenic mice. *Nature* **318**, 533–538 (1985).
41. Midelfort, K. S. *et al.* Substantial Energetic Improvement with Minimal Structural Perturbation in a High Affinity Mutant Antibody. *J. Mol. Biol.* **343**, 685–701 (2004).
42. Shultz, L. D., Brehm, M. A., Garcia-Martinez, J. V. & Greiner, D. L. Humanized mice for immune system investigation: progress, promise and challenges. *Nat. Rev. Immunol.* **12**, 786–798 (2012).
43. Medema, J. P. *et al.* Expression of the Serpin Serine Protease Inhibitor 6 Protects Dendritic Cells from Cytotoxic T Lymphocyte–Induced Apoptosis. *J. Exp. Med.* **194**, 657–668 (2001).
44. Peng, Q. *et al.* PD-L1 on dendritic cells attenuates T cell activation and regulates response to immune checkpoint blockade. *Nat Commun* **11**, 4835 (2020).
45. Gordon, K. S. *et al.* Screening for CD19-specific chimaeric antigen receptors with enhanced signalling via a barcoded library of intracellular domains. *Nat Biomed Eng* **6**, 855–866 (2022).
46. Melenhorst, J. J. *et al.* Decade-long leukaemia remissions with persistence of CD4+ CAR T cells. *Nature* **602**, 503–509 (2022).

908 47. Reinhard, K. *et al.* An RNA vaccine drives expansion and efficacy of claudin-CAR-T cells
909 against solid tumors. *Science* **367**, 446–453 (2020).
910 48. Long, A. H. *et al.* 4-1BB costimulation ameliorates T cell exhaustion induced by tonic signaling
911 of chimeric antigen receptors. *Nature Medicine* 1–13 (2015) doi:10.1038/nm.3838.
912 49. Ajina, A. & Maher, J. Strategies to Address Chimeric Antigen Receptor Tonic Signaling. *Mol.*
913 *Cancer Ther.* **17**, 1795–1815 (2018).
914 50. Gomes-Silva, D. *et al.* Tonic 4-1BB Costimulation in Chimeric Antigen Receptors Impedes T
915 Cell Survival and Is Vector-Dependent. *Cell Rep.* **21**, 17–26 (2017).
916 51. Gauthier, J. *et al.* Factors associated with outcomes after a second CD19-targeted CAR T-
917 cell infusion for refractory B-cell malignancies. *Blood* **137**, 323–335 (2021).
918 52. Myers, R. M. *et al.* Outcomes after Reinfusion of CD19-Specific Chimeric Antigen Receptor
919 (CAR)-Modified T Cells in Children and Young Adults with Relapsed/Refractory B-Cell Acute
920 Lymphoblastic Leukemia. *Blood* **138**, 474 (2021).
921 53. Wagner, D. L. *et al.* Immunogenicity of CAR T cells in cancer therapy. *Nat. Rev. Clin. Oncol.*
922 **18**, 379–393 (2021).
923 54. Faude, S. *et al.* Absolute lymphocyte count proliferation kinetics after CAR T-cell infusion
924 impact response and relapse. *Blood Adv.* **5**, 2128–2136 (2021).
925 55. Mackensen, A. *et al.* CLDN6-specific CAR-T cells plus amplifying RNA vaccine in relapsed or
926 refractory solid tumors: the phase 1 BNT211-01 trial. *Nat. Med.* **29**, 2844–2853 (2023).
927

Fig 1

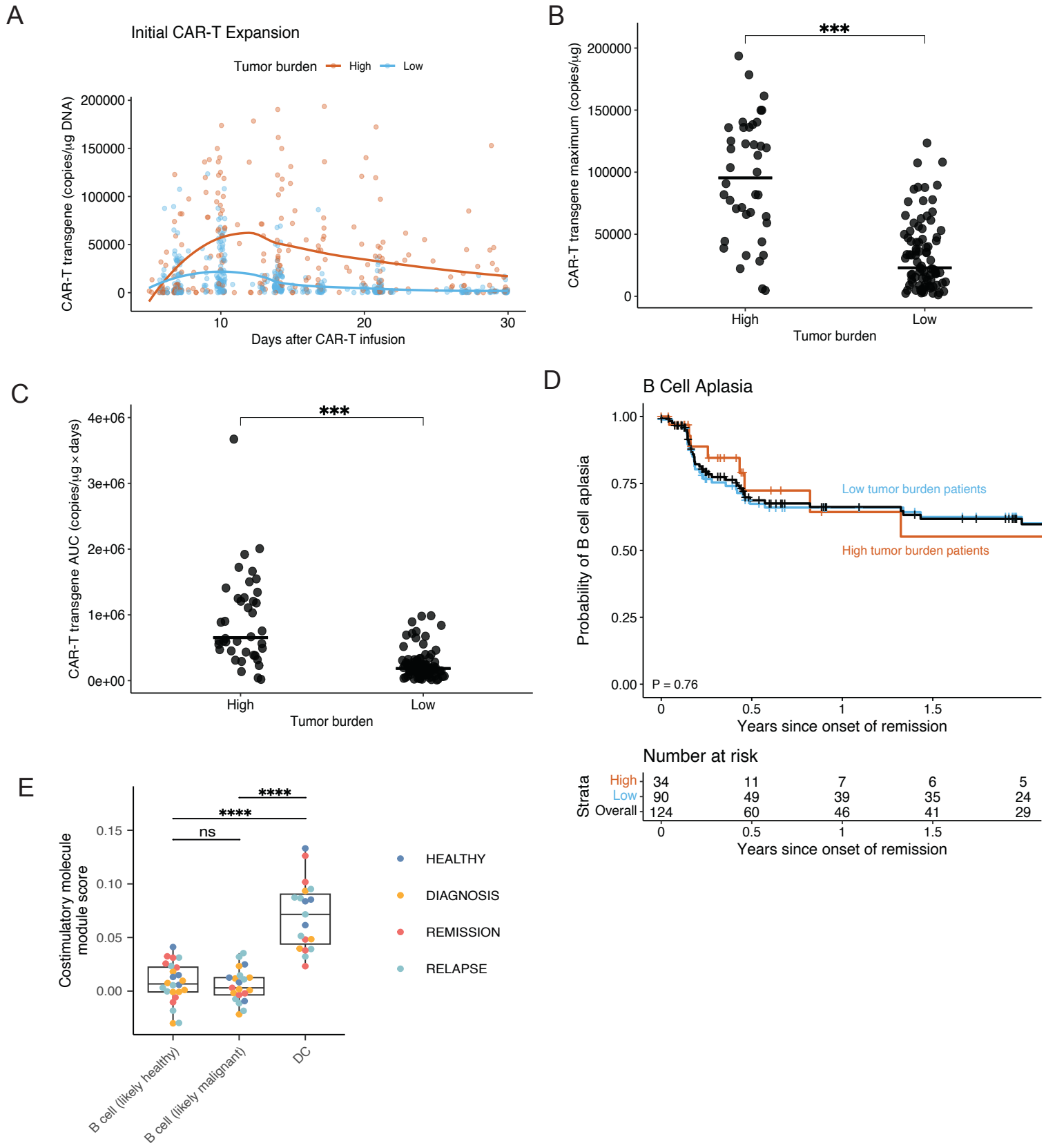
A
Initial CAR-T Expansion
Tumor burden
High
Low
CAR-T transgene (copies/μg DNA)
200000
150000
100000
50000
0
10
20
30
Days after CAR-T infusion
B
***
CAR-T transgene maximum (copies/μg)
200000
150000
100000
50000
0
High
Low
Tumor burden
C
***
CAR-T transgene AUC (copies/μg × days)
4e+06
3e+06
2e+06
1e+06
0e+00
High
Low
Tumor burden
D
B Cell Aplasia
Probability of B cell aplasia
1.00
0.75
0.50
0.25
0.00
Low tumor burden patients
High tumor burden patients
P = 0.76
0
0.5
1
1.5
Years since onset of remission
Number at risk
Strata
High 34 11 7 6 5
Low 90 49 39 35 24
Overall 124 60 46 41 29
0
0.5
1
1.5
Years since onset of remission
E
****
****
ns
Costimulatory molecule module score
0.15
0.10
0.05
0.00
B cell (likely healthy)
B cell (likely malignant)
DC
HEALTHY
DIAGNOSIS
REMISSION
RELAPSE

Fig 2

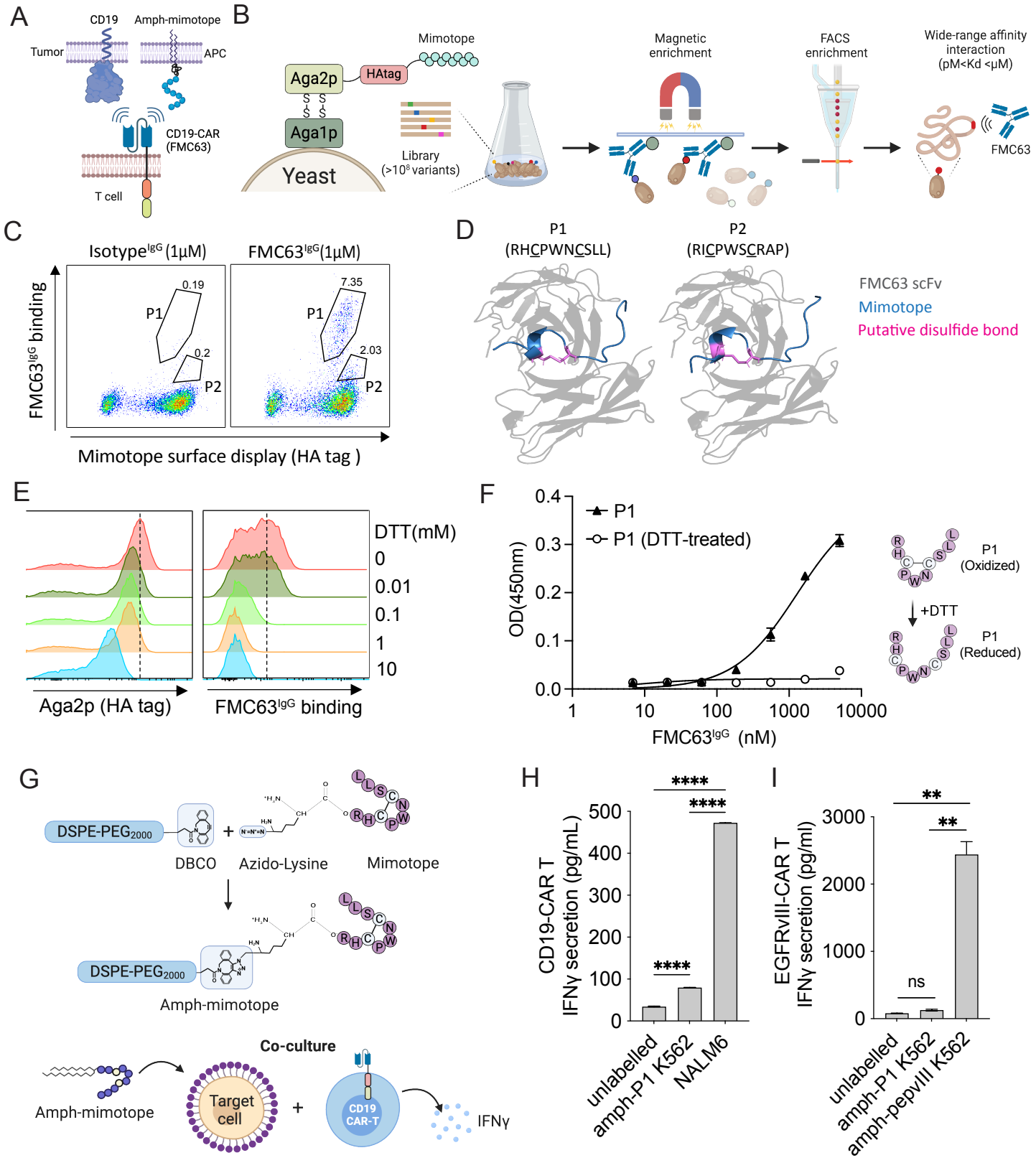
A
CD19
Amph-mimotope
Tumor
APC
CD19-CAR
(FMC63)
T cell
B
Mimotope
Aga2p
HAtag
Aga1p
Yeast
Library
(>10⁸ variants)
Magnetic
enrichment
FACS
enrichment
Wide-range affinity
interaction
(pM<Kd <μM)
FMC63
C
Isotype^IgG (1μM)
FMC63^IgG(1μM)
FMC63^IgG binding
P1
P2
0.19
0.2
7.35
2.03
Mimotope surface display (HA tag)
D
P1
(RHCPWNCSLL)
P2
(RICPWSCRAP)
FMC63 scFv
Mimotope
Putative disulfide bond
E
DTT(mM)
0
0.01
0.1
1
10
Aga2p (HA tag)
FMC63^IgG binding
F
P1
P1 (DTT-treated)
OD(450nm)
FMC63^IgG (nM)
P1
(Oxidized)
+DTT
P1
(Reduced)
G
DSPE-PEG2000
DBCO
Azido-Lysine
Mimotope
Amph-mimotope
Co-culture
Amph-mimotope
Target
cell
CD19
CAR-T
IFNγ
H
CD19-CAR T
IFNγ secretion (pg/mL)
unlabelled
amph-P1 K562
NALM6
I
EGFRvIII-CAR T
IFNγ secretion (pg/ml)
unlabelled
amph-P1 K562
amph-pepvIII K562
ns

Fig 3

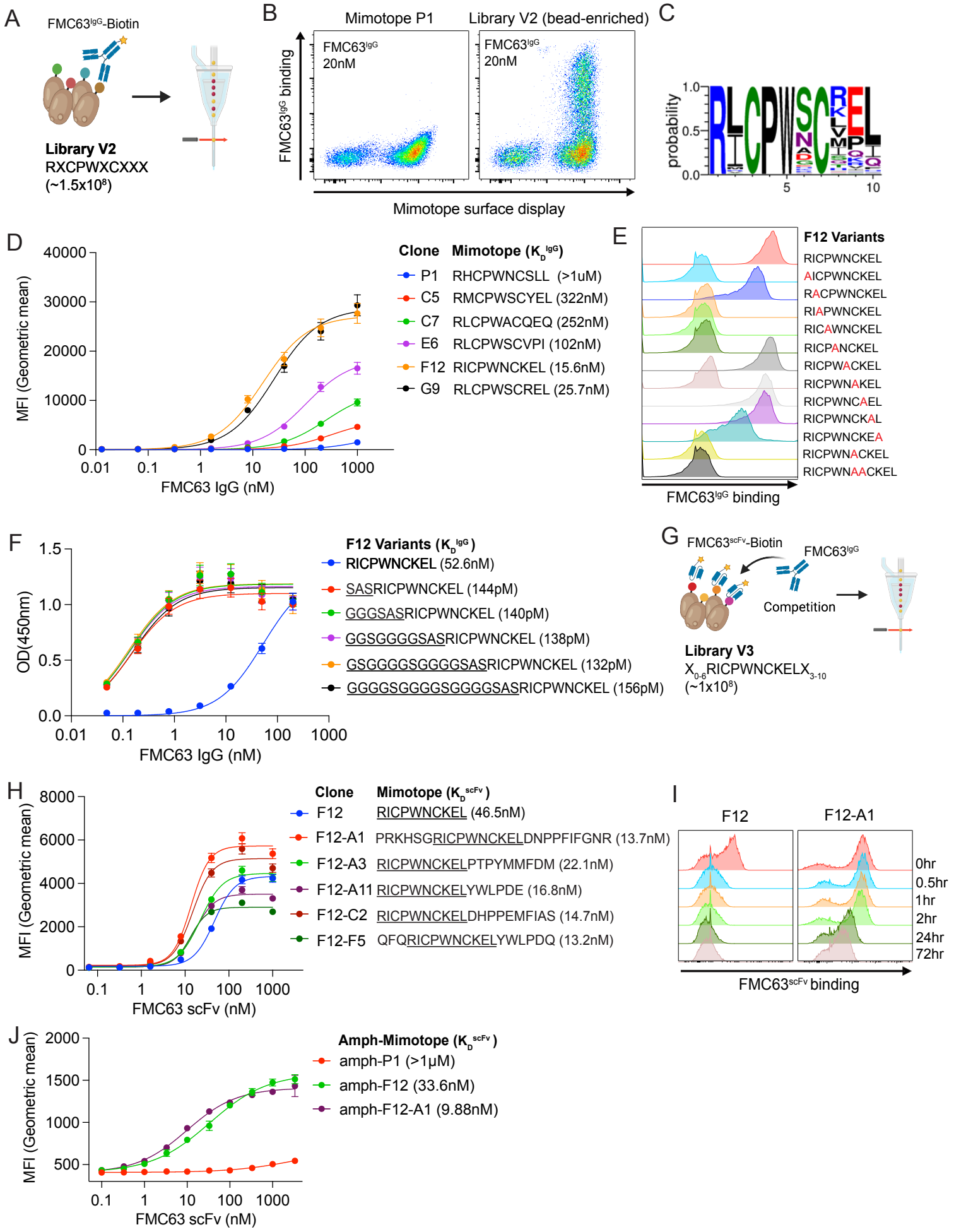
A
FMC63IgG-Biotin
Library V2
RXCPWXCXXX
(~1.5x10⁸)
B
Mimotope P1
Library V2 (bead-enriched)
FMC63IgG 20nM
FMC63IgG 20nM
FMC63IgG binding
Mimotope surface display
C
probability
1.0
0.5
0.0
5
10
D
MFI (Geometric mean)
FMC63 IgG (nM)
Clone Mimotope (KD IgG)
P1 RHCPWNCSLL (>1uM)
C5 RMCPWSCYEL (322nM)
C7 RLCPWACQEQ (252nM)
E6 RLCPWSCVPI (102nM)
F12 RICPWNCKEL (15.6nM)
G9 RLCPWSCREL (25.7nM)
E
F12 Variants
RICPWNCKEL
AICPWNCKEL
RACPWNCKEL
RIAPWNCKEL
RICAWNCKEL
RICPANCKEL
RICPWACKEL
RICPWNAKEL
RICPWNCAEL
RICPWNCKAL
RICPWNCKEA
RICPWNACKEL
RICPWNAACKEL
FMC63IgG binding
F
OD(450nm)
FMC63 IgG (nM)
F12 Variants (KD IgG)
RICPWNCKEL (52.6nM)
SASRICPWNCKEL (144pM)
GGGSASRICPWNCKEL (140pM)
GGSGGGGSASRICPWNCKEL (138pM)
GSGGGGSGGGGSASRICPWNCKEL (132pM)
GGGGSGGGGSGGGGSASRICPWNCKEL (156pM)
G
FMC63scFv-Biotin
FMC63IgG
Competition
Library V3
X0-6RICPWNCKELX3-10
(~1x10⁸)
H
MFI (Geometric mean)
FMC63 scFv (nM)
Clone Mimotope (KD scFv)
F12 RICPWNCKEL (46.5nM)
F12-A1 PRKHSGRICPWNCKELDNPPFIFGNR (13.7nM)
F12-A3 RICPWNCKELPTPYMMFDM (22.1nM)
F12-A11 RICPWNCKELYWLPDE (16.8nM)
F12-C2 RICPWNCKELDHPPEMFIAS (14.7nM)
F12-F5 QFQRICPWNCKELYWLPDQ (13.2nM)
I
F12
F12-A1
0hr
0.5hr
1hr
2hr
24hr
72hr
FMC63scFv binding
J
MFI (Geometric mean)
FMC63 scFv (nM)
Amph-Mimotope (KD scFv)
amph-P1 (>1μM)
amph-F12 (33.6nM)
amph-F12-A1 (9.88nM)

Fig 4

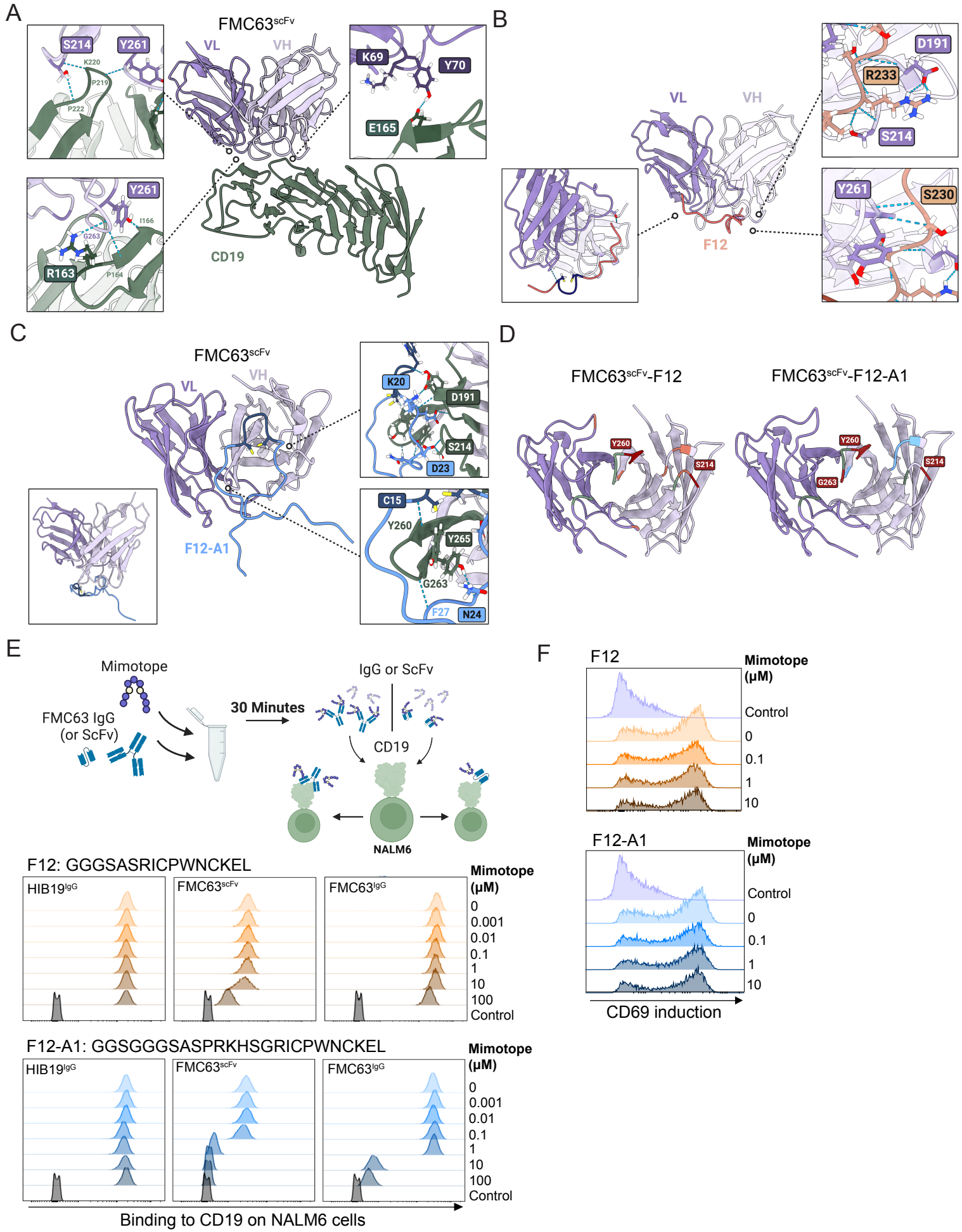
A
FMC63scFv
VL
VH
S214
Y261
K220
P219
P222
K69
Y70
E165
Y261
I166
G263
R163
P164
CD19
B
VL
VH
D191
R233
S214
Y261
S230
F12
C
FMC63scFv
VL
VH
K20
D191
S214
D23
F12-A1
C15
Y260
Y265
G263
F27
N24
D
FMC63scFv-F12
FMC63scFv-F12-A1
Y260
S214
Y260
G263
S214
E
Mimotope
FMC63 IgG
(or ScFv)
30 Minutes
IgG or ScFv
CD19
NALM6
F12: GGGSASRICPWNCKEL
HIB19IgG
FMC63scFv
FMC63IgG
Mimotope
(μM)
0
0.001
0.01
0.1
1
10
100
Control
F12-A1: GGSGGGSASPRKHSGRICPWNCKEL
HIB19IgG
FMC63scFv
FMC63IgG
Mimotope
(μM)
0
0.001
0.01
0.1
1
10
100
Control
Binding to CD19 on NALM6 cells
F
F12
Mimotope
(μM)
Control
0
0.1
1
10
F12-A1
Mimotope
(μM)
Control
0
0.1
1
10
CD69 induction

Fig 5

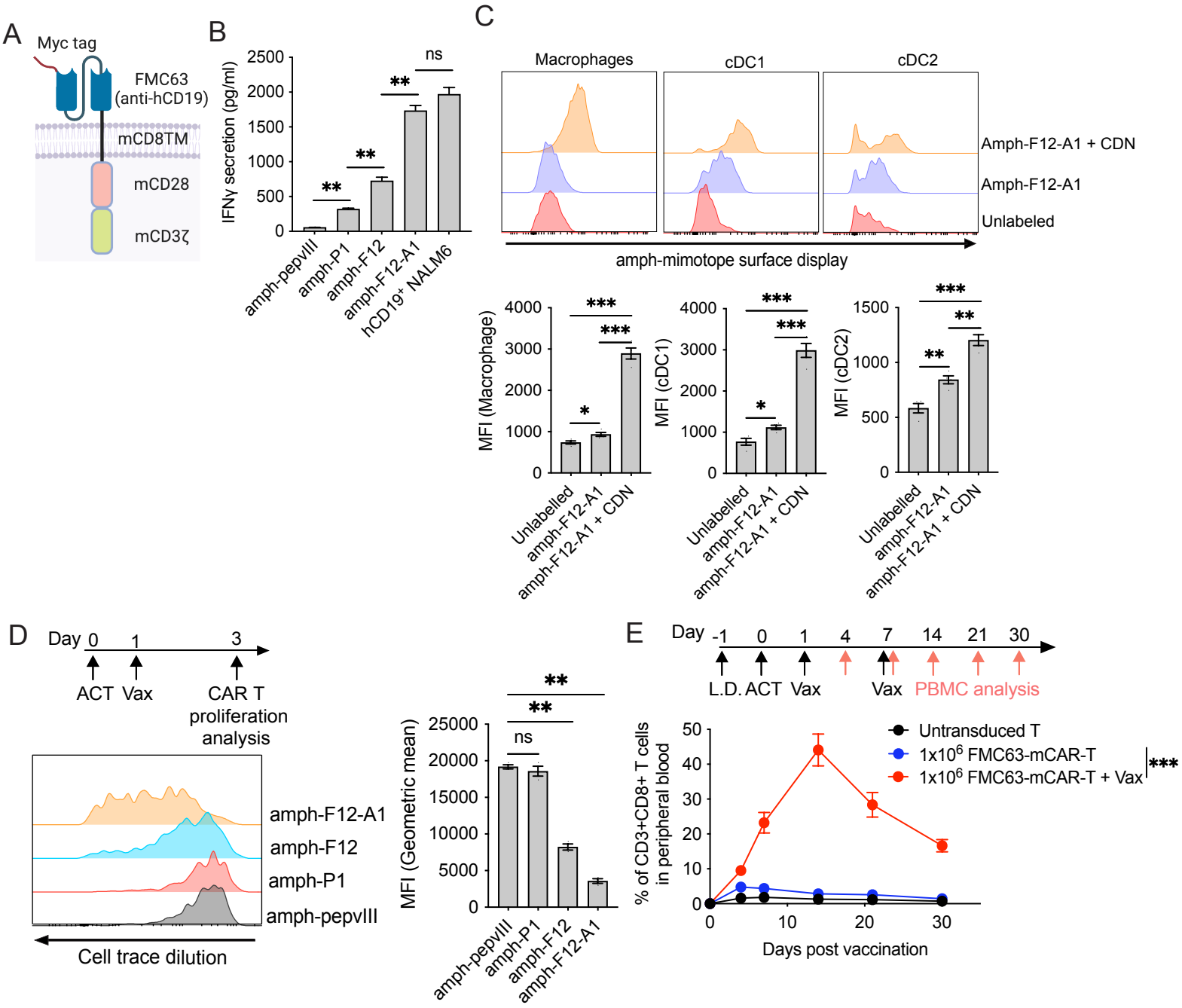
A
Myc tag
FMC63
(anti-hCD19)
mCD8TM
mCD28
mCD3ζ
B
IFNγ secretion (pg/ml)
2500
2000
1500
1000
500
0
ns
**
**
**
amph-pepvIII
amph-P1
amph-F12
amph-F12-A1
hCD19+ NALM6
C
Macrophages
cDC1
cDC2
Amph-F12-A1 + CDN
Amph-F12-A1
Unlabeled
amph-mimotope surface display
MFI (Macrophage)
MFI (cDC1)
MFI (cDC2)
4000
3000
2000
1000
0
1500
1000
500
***
***
*
**
Unlabelled
amph-F12-A1
amph-F12-A1 + CDN
D
Day 0 1 3
ACT Vax
CAR T
proliferation
analysis
amph-F12-A1
amph-F12
amph-P1
amph-pepvIII
Cell trace dilution
MFI (Geometric mean)
25000
20000
15000
10000
5000
0
**
**
ns
amph-pepvIII
amph-P1
amph-F12
amph-F12-A1
E
Day -1 0 1 4 7 14 21 30
L.D. ACT Vax
Vax PBMC analysis
% of CD3+CD8+ T cells
in peripheral blood
50
40
30
20
10
0
Untransduced T
1x10^6 FMC63-mCAR-T
1x10^6 FMC63-mCAR-T + Vax
***
0
10
20
30
Days post vaccination

Fig 6

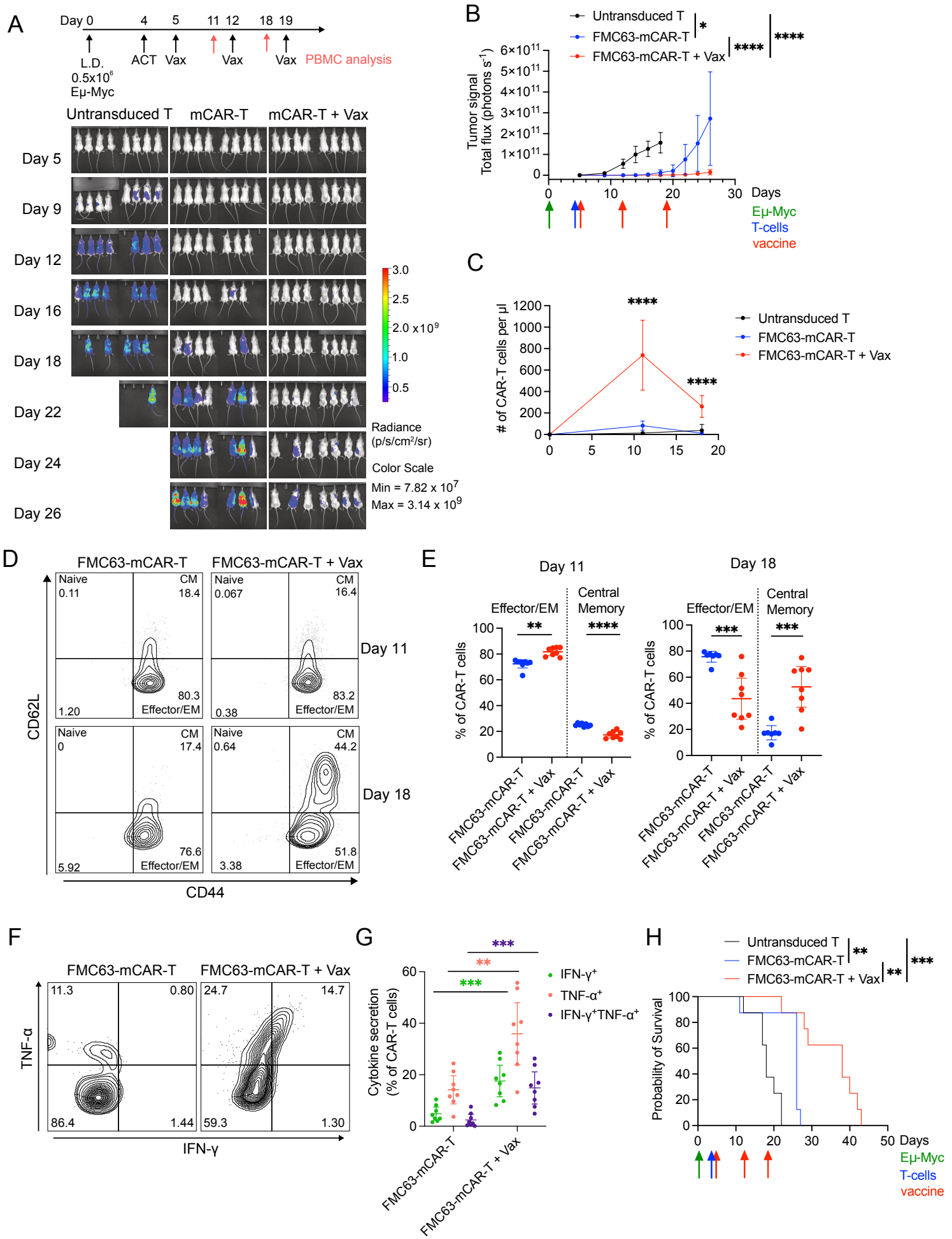
A
Day 0
4
5
11 12
18 19
L.D.
0.5x10^6
Eμ-Myc
ACT
Vax
Vax
Vax
PBMC analysis
Untransduced T
mCAR-T
mCAR-T + Vax
Day 5
Day 9
Day 12
Day 16
Day 18
Day 22
Day 24
Day 26
3.0
2.5
2.0 x10^9
1.0
0.5
Radiance
(p/s/cm²/sr)
Color Scale
Min = 7.82 x 10^7
Max = 3.14 x 10^9
B
Untransduced T
FMC63-mCAR-T
FMC63-mCAR-T + Vax
Tumor signal
Total flux (photons s^-1)
Days
Eμ-Myc
T-cells
vaccine
C
# of CAR-T cells per μl
Untransduced T
FMC63-mCAR-T
FMC63-mCAR-T + Vax
D
FMC63-mCAR-T
FMC63-mCAR-T + Vax
Naive
CM
Effector/EM
Day 11
Day 18
CD62L
CD44
E
Day 11
Day 18
Effector/EM
Central Memory
% of CAR-T cells
FMC63-mCAR-T
FMC63-mCAR-T + Vax
F
FMC63-mCAR-T
FMC63-mCAR-T + Vax
TNF-α
IFN-γ
G
Cytokine secretion
(% of CAR-T cells)
IFN-γ+
TNF-α+
IFN-γ+TNF-α+
FMC63-mCAR-T
FMC63-mCAR-T + Vax
H
Untransduced T
FMC63-mCAR-T
FMC63-mCAR-T + Vax
Probability of Survival
Days
Eμ-Myc
T-cells
vaccine

Fig 7

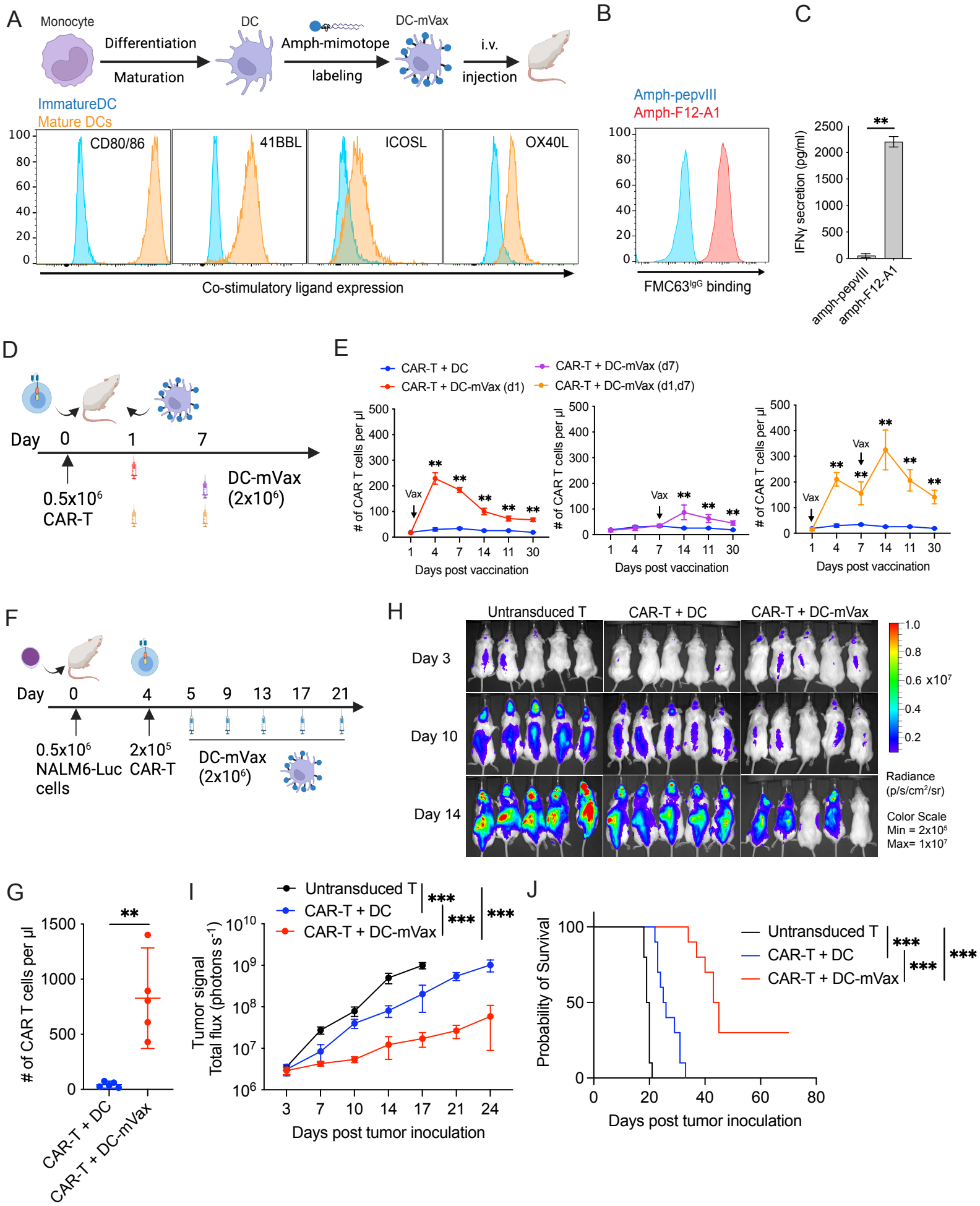
A
Monocyte
Differentiation
Maturation
DC
Amph-mimotope
labeling
DC-mVax
i.v.
injection
ImmatureDC
Mature DCs
CD80/86
41BBL
ICOSL
OX40L
Co-stimulatory ligand expression
B
Amph-pepvIII
Amph-F12-A1
FMC63IgG binding
C
IFNγ secretion (pg/ml)
amph-pepvIII
amph-F12-A1
D
Day 0 1 7
0.5x10⁶ CAR-T
DC-mVax (2x10⁶)
E
CAR-T + DC
CAR-T + DC-mVax (d1)
CAR-T + DC-mVax (d7)
CAR-T + DC-mVax (d1,d7)
# of CAR T cells per µl
Vax
Days post vaccination
F
Day 0 4 5 9 13 17 21
0.5x10⁶ NALM6-Luc cells
2x10⁵ CAR-T
DC-mVax (2x10⁶)
H
Untransduced T
CAR-T + DC
CAR-T + DC-mVax
Day 3
Day 10
Day 14
Radiance (p/s/cm²/sr)
Color Scale
Min = 2x10⁵
Max= 1x10⁷
G
# of CAR T cells per µl
CAR-T + DC
CAR-T + DC-mVax
I
Untransduced T
CAR-T + DC
CAR-T + DC-mVax
Tumor signal Total flux (photons s⁻¹)
Days post tumor inoculation
J
Probability of Survival
Untransduced T
CAR-T + DC
CAR-T + DC-mVax
Days post tumor inoculation